Microbiome

RESEARCH

Open Access

Pathobionts from chemically disrupted gut microbiota induce insulin-dependent diabetes in mice

Xin Yang[1], Zhiyi Wang[1], Junling Niu[1,2], Rui Zhai[1], Xinhe Xue[1], Guojun Wu[3], Yuanyuan Fang[4], Guangxun Meng[2], Huijuan Yuan[4], Liping Zhao[1,3*] and Chenhong Zhang[1*]

Abstract

Background Dysbiotic gut microbiome, genetically predisposed or chemically disrupted, has been linked with insulin-dependent diabetes (IDD) including autoimmune type 1 diabetes (T1D) in both humans and animal models. However, specific IDD-inducing gut bacteria remain to be identified and their casual role in disease development demonstrated via experiments that can fulfill Koch's postulates.

Results Here, we show that novel gut pathobionts in the Muribaculaceae family, enriched by a low-dose dextran sulfate sodium (DSS) treatment, translocated to the pancreas and caused local inflammation, beta cell destruction and IDD in C57BL/6 mice. Antibiotic removal and transplantation of gut microbiota showed that this low DSS disrupted gut microbiota was both necessary and sufficient to induce IDD. Reduced butyrate content in the gut and decreased gene expression levels of an antimicrobial peptide in the pancreas allowed for the enrichment of selective members in the Muribaculaceae family in the gut and their translocation to the pancreas. Pure isolate of one such members induced IDD in wildtype germ-free mice on normal diet either alone or in combination with normal gut microbiome after gavaged into stomach and translocated to pancreas. Potential human relevance of this finding was shown by the induction of pancreatic inflammation, beta cell destruction and IDD development in antibiotic-treated wildtype mice via transplantation of gut microbiome from patients with IDD including autoimmune T1D.

Conclusion The pathobionts that are chemically enriched in dysbiotic gut microbiota are sufficient to induce insulin-dependent diabetes after translocation to the pancreas. This indicates that IDD can be mainly a microbiome-dependent disease, inspiring the need to search for novel pathobionts for IDD development in humans.

Keywords Insulin-dependent diabetes, Gut pathobionts, Muribaculaceae

*Correspondence:
Liping Zhao
lpzhao@sjtu.edu.cn; liping.zhao@rutgers.edu
Chenhong Zhang
zhangchenhong@sjtu.edu.cn
[1] State Key Laboratory of Microbial Metabolism and Ministry of Education Key Laboratory of Systems Biomedicine, School of Life Sciences and Biotechnology, Shanghai Jiao Tong University, Shanghai 200240, China
[2] The Center for Microbes, Development and Health, CAS Key Laboratory of Molecular Virology & Immunology, Institute Pasteur of Shanghai, University of Chinese Academy of Sciences, Shanghai 200031, China
[3] Department of Biochemistry and Microbiology and New Jersey Institute for Food, Nutrition, and Health, School of Environmental and Biological Sciences, Rutgers University, New Brunswick, NJ 08901, USA
[4] Department of Endocrinology of Henan Provincial People's Hospital, People's Hospital of Zhengzhou University, Zhengzhou 450003, Henan, China

Background

Insulin-dependent diabetes (IDD) refers to a wide range of diabetic conditions characterized by absolute insufficiency of insulin secretion [1]. The most prevalent type of IDD is type 1 diabetes (T1D), which is an autoimmune condition that leads to specific destruction of beta cells and complete loss of insulin-production [2]. Except autoimmune T1D in which genetics may play a critical role, IDD can be caused by environmental factors, such as treatment with immune checkpoint inhibitors, toxic compounds, and infection etc. [3–5]. The rapid increase in the incidence of IDD in the past three decades indicates that environmental factors, rather than genetics, may be the main driver of such diseases [6]. However, the pathological mechanism on how such environmental factors can induce IDD remain elusive.

It has been hypothesized that gut microbiota may work as a mediating factor in the development of IDD [6]. This hypothesis has been supported mainly by studies on the role of gut microbiota in the development of T1D in both animal models and human cohorts [7]. Altered gut microbiota in connection to T1D has been reported in Finnish, German, Italian, Mexican, American (Colorado) and Turkish children [8–10]. The longitudinal functional profiling of the developing gut microbiome of infants in TEDDY study showed that short-chain fatty acids (SCFAs) from fermentation of gut microbiota have protective effects in early-onset human T1D [8]. Studies have shown that the gut microbiota and its metabolites contribute to the development of T1D in NOD mice through regulating toll-like receptor-dependent signaling [11, 12], sex hormone-related pathways [13], IL-17 related mucosal immune reactions [14, 15], and pancreatic production of antimicrobial peptides [16]. However, germ-free mice derived from NOD mice can still develop T1D, indicating that the gut microbiota is not essential for the development of T1D in this animal model [13]. The development of IDD in mice treated with toxic compounds, such as streptozotocin (STZ), has also been associated with gut microbiota dysbiosis. Interestingly, the depletion of the gut microbiota by an antibiotic cocktail blocked IDD induction by STZ, showing that the gut microbiota may be indispensable for this chemically-induced IDD [7]. However, specific members of the dysbiotic gut microbiota which may drive IDD, and the associated etiological mechanisms remain to be elucidated.

Many toxic compounds have been shown to disrupt the gut microbiota and aggravate inflammation-related diseases, including metabolic diseases [17]. Notably, dextran sulfate sodium (DSS), a compound with very low bioavailability, has been well known for its effect on disrupting the gut microbiota and inducing acute colitis at a high dose (2-3%) and chronic colitis at a low dose (0.5-1%) when administered via drinking water in mice [18–20]. To explore how an even lower level of DSS would affect the gut microbiota and host health, we reduced the dose to 0.2%. We serendipitously found that the mice did not show inflammation or impaired barrier function in their gut; instead, they developed IDD with pancreatic beta cells significantly destructed. We identified and isolated one of the pathobionts in family Muribaculaceae which was enriched in the low DSS-disrupted gut microbiota and confirmed that this single pathobiont is sufficient to induce the initiation and progression of IDD in germfree mice. This study indicates that IDD can be a microbiome-dependent disease, inspiring the search of such novel pathobionts for IDD development in humans.

Results

Low-dose DSS induced gut microbiota-dependent IDD

To determine how a lower than usual dose of DSS would affect gut microbiota and host health, we randomized 6-week-old C57BL/6 mice into a treatment group with 0.2% DSS in the drinking water or a control group with no any DSS intake. Compared with control mice, the mice that received 12 weeks of low dose DSS treatment showed a significant increase in blood glucose levels and decrease in insulin levels in oral glucose tolerance test (OGTT) (Fig. 1A and B). Moreover, the low dose DSS-treated mice and control did not differ in blood glucose levels in an insulin tolerance test (ITT), indicating that the low dose DSS-treated group did not develop insulin resistance (Fig. 1C). Compared with the control mice, low dose DSS-treated mice had significantly decreased insulin expression in the pancreas (Fig. 1D). We also found that the fasting C-peptide level in serum was significantly lower in mice with low dose DSS treatment than the control mice, demonstrating that the abnormal high glucose level was due to low insulin production and secretion (Figure S1). The low dose DSS-treated mice showed islet destruction in the pancreas (Fig. 1E). These mice also showed mild pancreatitis, as indicated by histological characteristics, such as inflammatory cell infiltration and edema in the pancreas (Fig. 1F), and an increase in serum amylase levels (Figure S2). The DSS-treated mice had significantly higher daily food and water intake than the control mice starting from the 8th week of treatment (Figure S3). However, the energy consumption, body weight gain, and lipid metabolism did not differ between low dose DSS treatment and control throughout the study period (Figures S4). Thus, the treatment with 0.2% DSS in drinking water induced IDD in wild-type C57BL/6 mice.

However, unlike higher doses DSS [21], this low dose DSS treatment did not induce colitis or gut barrier impairment in mice. H&E-stained histological sections

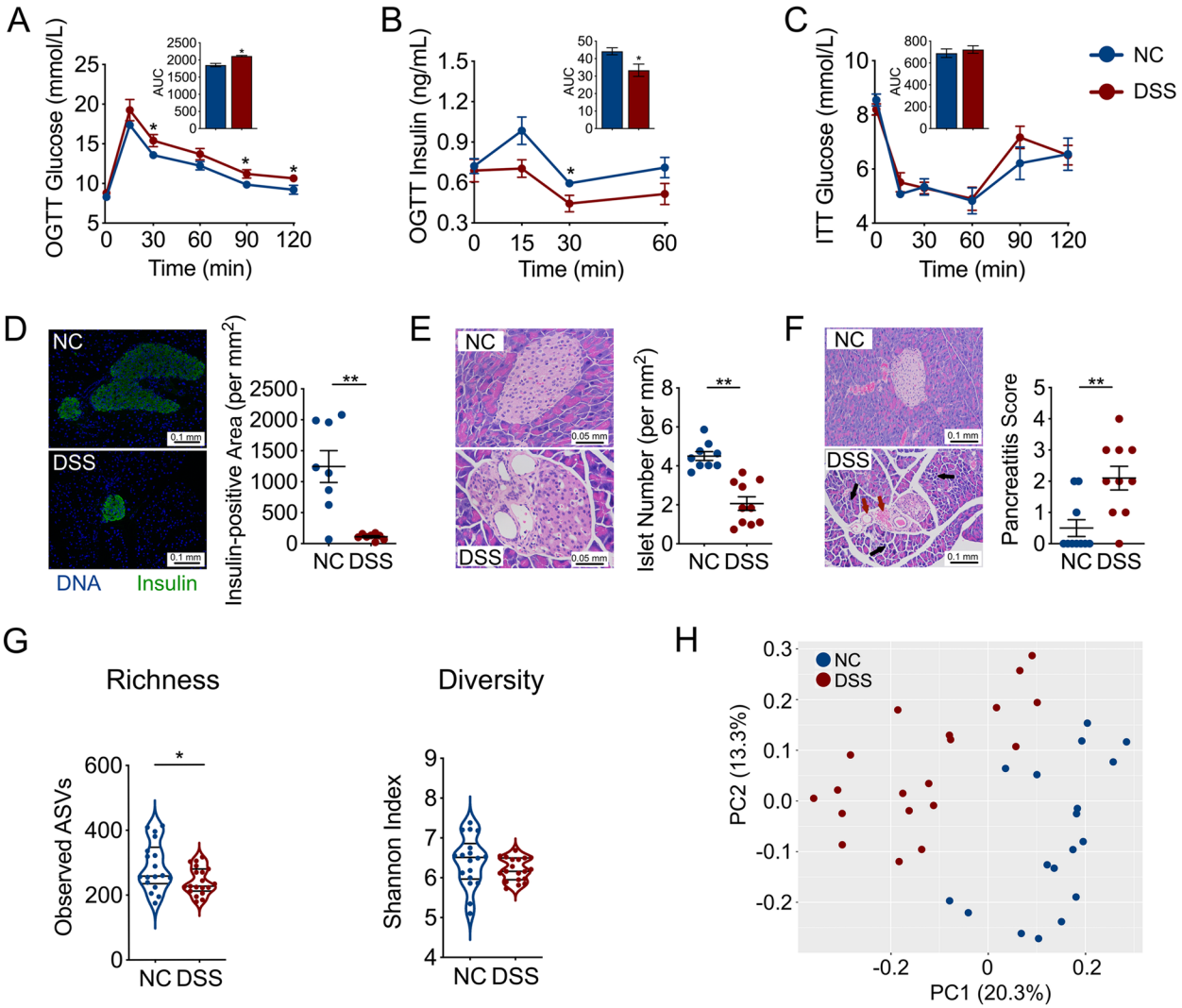

Fig. 1 IDD induced by 0.2% DSS treatment in mice **A** Blood glucose and **B** insulin levels of normal control (NC) and DSS-treated mice, as measured by an oral glucose tolerance test (OGTT) (the area under the curve (AUC) is shown in the inset panels). NC group, *n*=9; DSS group, *n*=7. **C** Blood glucose levels of NC and DSS-treated mice as measured by an insulin tolerance test (ITT) (the AUC is shown in the inset panels). NC group, *n*=8; DSS group, *n*=9. **D** Histological sections of pancreatic tissue (200×, scale bar = 0.1 mm) from NC and DSS-treated mice stained for insulin (green) and DNA (blue), and the insulin-positive area was quantified (at right). NC group, *n*=8; DSS group, *n*=8. **E** The number of islets per mm^2 of pancreatic tissue was calculated based on H&E-stained histological sections of pancreatic tissue (400×, scale bar = 0.05 mm) from NC and DSS-treated mice. NC group, *n*=9; DSS group, *n*=10. **F** The histologic pancreatitis score was evaluated by edema, inflammation, and vacuolization in the H&E-stained histological sections of pancreatic tissue (200×, scale bar = 0.1 mm) from NC and DSS-treated mice. Black arrows, scattered structure; Red arrows, increased peri-islet neovascularization. NC group, *n*=10; DSS group, *n*=10. **G** The alpha-diversity of gut microbiota in NC and DSS-treated mice. **H** Overall gut microbial structure in NC and DSS-treated mice. Principal coordinate analysis (PCoA) was performed on the basis of Bray-Curtis distance at the amplicon sequence variant (ASV) level. For (**G**) and (**H**), NC group, *n*=17; DSS group, *n*=18. The data in (**A**)-(**F**) are shown as the mean ± SEM, and Student's t-test (two-tailed) was used to analyze difference between NC and DSS groups. **P* <0.05 and ***P* <0.01. NC, control mice provided pure drinking water; DSS, mice treated with 0.2% (w/v) DSS in drinking water

of colon tissue showed that there were no structural changes of epithelium in the mice with 0.2% DSS in drinking water compared with the control (Figure S5). The fluorescein isothiocyanate (FITC)-dextran test, levels of mRNA expression of 8 different genes related with gut barrier integrity and immunohistochemical staining of Occludin and Zo-1 showed no significant difference in intestinal permeability in mice with or without 0.2% DSS treatment (Figure S5). Moreover, the fecal lipocalin-2 content, a biomarker for gut inflammation, had no significant difference between the 0.2% DSS-treated and control mice (Figure S5).

Although the dose of DSS used in our model was much lower than the dose needed to induce colitis [18], the gut microbiota structure in the low dose DSS-treated mice was significantly shifted away from the control, as shown by its reduced richness (Fig. 1G) and significant difference in principal coordinate analysis (PCoA) score plot of Bray-Curtis distance based on the amplicon sequence variants (ASVs) of the 16S rRNA gene V3-V4 region (P=0.001 by permutational multivariate analysis of variance (PERMANOVA) test with 999 permutations, Fig. 1H). Thus, without altering bacterial load (Figure S6), the development of low dose DSS-induced IDD in mice was accompanied by significant changes in the gut microbiota without inducing colitis.

To find out whether the disrupted gut microbiota was necessary for the development of IDD induced by low dose DSS, we treated the adult C57BL/6 mice with a cocktail of antibiotics for 5 weeks that depleted the gut microbiota by more than 99% (Figure S7). We then introduced 0.2% DSS into the drinking water of the mice which were continuously treated with the antibiotic cocktail. Under the gut microbiota-depleted condition, DSS-treated (ABX_{DSS}) and control (ABX_{NC}) mice had indistinguishable glucose metabolism, insulin secretion and histology in the pancreas (Fig. 2, Figure S2). Thus, the removal of the gut microbiota abolished the low dose DSS-induced IDD in mice, indicating that the gut microbiota is essential for the disease induction. To test if the DSS-disrupted gut microbiota is sufficient to induce IDD, we transferred feces from control and 0.2% DSS-treated C57BL/6 mice to antibiotic-treated mice [22]. The recipient mice were denoted FM_{NC} and FM_{DSS} mice, respectively. Two weeks after the transplantation, the FM_{DSS} and FM_{NC} mice developed a gut microbiota more similar to those of their donor (Figure S8). Moreover, the FM_{DSS} mice showed significantly higher blood glucose level, lower insulin secretion, more beta cell destruction and more signs of pancreatitis compared with the FM_{NC} mice, even though all the recipient mice were provided pure water during the trial (Fig. 2, Figure S2). This result demonstrates that the gut microbiota treated by low dose DSS is sufficient to induce IDD in mice. Thus, this chemically induced IDD in mice was causally mediated by the gut microbiota which was disrupted by the low dose DSS treatment.

Translocation of candidate gut pathobionts to the pancreas promoted local inflammation

To identify key members of the gut microbiota enriched by the low dose DSS which may causally contribute to IDD development, we first identified ASVs in the gut microbiota which showed significant differences between the 0.2% DSS-treated and control mice by sparse partial least squares discriminant analysis (sPLS-DA) (Fig. 3A and Figure S8). Notable changes were observed in the family Muribaculaceae (phylum Bacteroidota), a major but understudied mouse taxon [23]. Specifically, 4 ASVs in this family were enriched, while 6 ASVs were depleted (Fig. 3A). On the other hand, ASVs associated with potential butyrate producers, such as 2 ASVs in the genus *Eubacterium*, were decreased (Fig. 3A). Butyrate content was significantly lower in DSS-treated than in control mice (Fig. 3B). The butyrate content was also significantly lower in FM_{DSS} mice compared with that in FM_{NC} mice (Fig. 3B). Reduced diversity of butyrate-producing bacteria and lower gut butyrate content have been linked with overgrowth of pathobionts [24]. We hypothesized that the 4 ASVs in the family Muribaculaceae enriched by low dose DSS may represent candidate pathobionts for IDD development.

Translocation of gut pathobionts to pancreas has bene linked with a few disease conditions [25]. We hypothesized that the candidate pathobionts enriched in low dose DSS disrupted gut microbiota may translocate to pancreas and induce IDD. Indeed, qPCR and fluorescence in situ hybridization (FISH) targeting the 16S rRNA gene showed that the bacterial load was significantly higher (by at least one order of magnitude) in the pancreas of the low dose DSS-treated and FM_{DSS} mice than in that of their respective controls (Fig. 3C and D, Figure S10 and S11). Absolute abundance by multiplying the relative abundance from sequencing the V3-V4 region of the 16S rRNA gene of the microbiota with qPCR derived total copy number of 16S rRNA genes in the pancreas showed that the most abundant bacteria in the pancreas of control mice belonged to the family Akkermansiaceae, but the most abundant of microbiota in the pancreas of low dose DSS-treated mice was the family Muribaculaceae, which was 1.44 times that of the family Akkermansiaceae (Fig. 3E). Notably, the 4 ASVs (ASV 2778, ASV 6220, ASV 6451 and ASV 6263) in Muribaculaceae, which were significantly enriched in the gut by 0.2% DSS treatment (Fig. 3A), also showed a trend of being enriched in the pancreas of the low dose DSS-treated mice (Fig. 3F). Other ASVs in the same family showed no difference in pancreas between the low dose DSS-treated and control mice. The bacterial load was not increased in the liver of the low dose DSS-treated mice (Figure S12), suggesting that the gut microbiota specifically translocated to the pancreas. Reduced production of cathelicidin-related antimicrobial peptide (CRAMP) by pancreatic beta cells has been linked with the development of autoimmunity in the pancreas and T1D [16]. We found that the expression of the *Cramp* gene in the pancreas of 0.2% DSS-treated mice and FM_{DSS} mice was significantly lower than that in the pancreas of their respective controls (Fig. 3G). The reduced antimicrobial peptide production

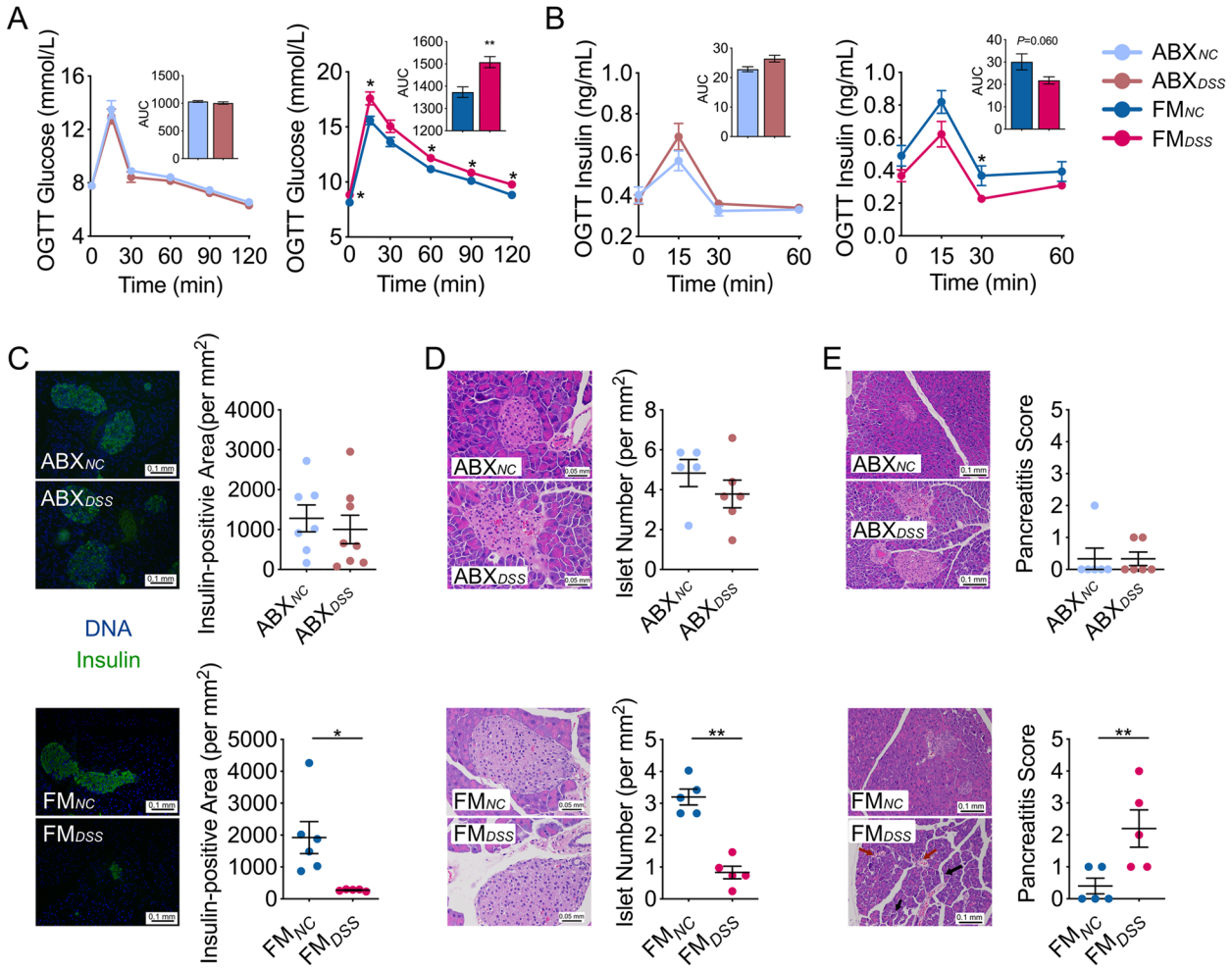

Fig. 2 The gut microbiota disrupted by 0.2% DSS was both necessary and sufficient for inducing IDD. **A** Blood glucose and **B** insulin levels with the AUC in the OGTT of ABX_{NC}, ABX_{DSS}, FM_{DSS} and FM_{NC} mice. For (**A**), ABX_{NC} group, n=10; ABX_{DSS} group, n=8; FM_{NC} group, n=8; FM_{DSS} group, n=8. For (**B**), ABX_{NC} group, n=9; ABX_{DSS} group, n=7; FM_{NC} group, n=6; FM_{DSS} group, n=6. **C** Histological sections of pancreatic tissue (200×, scale bar = 0.1 mm) from ABX_{NC}, ABX_{DSS}, FM_{DSS} and FM_{NC} mice stained for insulin (green) and DNA (blue), and the insulin-positive area was quantified (at bottom). ABX_{NC} group, n=7; ABX_{DSS} group, n=8; FM_{NC} group, n=6; FM_{DSS} group, n=5. **D** The number of islets per mm^2 of pancreatic tissue was calculated based on H&E-stained histological sections of pancreatic tissue (400×, scale bar = 0.05 mm) from ABX_{NC}, ABX_{DSS}, FM_{DSS} and FM_{NC} mice. ABX_{NC} group, n=5; ABX_{DSS} group, n=6; FM_{NC} group, n=5; FM_{DSS} group, n=5. **E** The histologic pancreatitis score was evaluated by edema, inflammation, and vacuolization in H&E-stained histological sections of pancreatic tissue (200×, scale bar = 0.1 mm) from ABX_{NC}, ABX_{DSS}, FM_{DSS} and FM_{NC} mice. Black arrows, scattered structure; Red arrows, increased peri-islet neovascularization. ABX_{NC} group, n=6; ABX_{DSS} group, n=6; FM_{NC} group, n=5; FM_{DSS} group, n=5. The data in (**A**)-(**E**) are shown as the mean ± SEM, and Student's t-test (two-tailed) was used to analyze the following pairs of groups: ABX_{NC} vs. ABX_{DSS}, or FM_{NC} vs. FM_{DSS}. *P <0.05 and **P <0.01. ABX_{NC}, antibiotic cocktail-treated mice provided pure water; ABX_{DSS}, antibiotic cocktail-treated mice treated with 0.2% (w/v) DSS added to drinking water; FM_{NC}, antibiotic cocktail-treated mice inoculated with the fecal microbiota from mice in the NC group and provided pure water; FM_{DSS}, antibiotic cocktail-treated mice inoculated with the fecal microbiota from mice in the DSS group and provided pure water

may have allowed bacterial overgrowth in pancreas. This may be one of the important reasons why the low dose DSS enriched ASVs in the gut microbiota translocated to and overgrew in pancreas.

We then examined immune responses of pancreas to the bacterial translocation and overgrowth. Infiltration of macrophages and total T cells were higher in the pancreas of the low dose DSS-treated mice than control (Fig. 3H). T cell differentiation toward $CD4^+$ and $CD8^+$ T cells were also higher in low dose DSS-treated mice than control, which may contribute to more inflammatory tissue damage [26]. Moreover, the low dose DSS-treated mice had a decreased population of regulatory T (T_{reg}) cells, which suppress the pathological immune response [27], suggesting a continued inflammatory pancreatic milieu (Fig. 3H). These immune responses were

also observed in FM_{DSS} mice but not in FM_{NC} mice (Figure S13). ABX_{DSS} and ABX_{NC} mice exhibited no detectable pancreatic bacterial loads via qPCR and FISH and no differences in immune responses (Figure S14). Taken together, our data supports the hypothesis that the downregulation of the pancreatic antimicrobial peptide CRAMP may allow more bacteria to translocate from the gut to the pancreas and overgrew there, which may lead to immune tolerance disruption and IDD development.

A pathobiont isolate from the family Muribaculaceae induced IDD in germfree mice

Based on above findings, we hypothesized that specific bacteria represented by the 4 ASVs in the family Muribaculaceae, which were enriched in both the gut and pancreas, might represent the key mediators of low dose DSS-induced IDD. To further examine the causal role of the bacteria in this family which were associated with low dose DSS-induced IDD, we first aimed to obtain their pure cultures from fresh feces of the low dose DSS-treated mice. Although bacteria in Muribaculaceae are dominant in the mouse gut microbiota, they had not been cultured until recently [23]. After sequence-guided screening of 13,079 colonies isolated using 46 different types of media (Table S1), we obtained a pure culture (named strain MF 13079) and its finished genomic sequence (Fig. 4A and B). The genome of the strain MF 13079 had two different 16S rRNA genes, each of which had 100% identity in the V3-V4 region with ASV 6263 and ASV 6451 respectively (Figure S15). These two ASVs were members of the family Muribaculaceae, which were among the 4 ASVs enriched in both the gut and pancreas of low dose DSS-treated mice (Fig. 3A). The nearest neighbor of MF 13079 in GenBank is *Duncaniella freteri* strain TLL-A3 but with only 93.7% homology in 16S rRNA gene sequence (Fig. 4C). The average nucleotide identity (ANI) values between the genome of strain MF 13079 and all 10 publicly available genomes of Muribaculaceae in GenBank ranged from 73.3% to 75.1%. Thus, MF 13079 may represent a new genus in Muribaculaceae [28]. Moreover, we found the genes for protecting against oxidative damage (COG0605 superoxide reductase, COG0753 catalase, COG0492 thioredoxin reductase, COG0450/COG2077/COG1225 peroxiredoxin) and genes for adhesion and immune evasion (COG0133/COG0159 tryptophan synthase) in the genome of MF 13079 (Table S2). Such genes may facilitate the overgrowth of this gut bacterium in the pancreas and qualify it as a pathobiont [29].

To test if MF 13079 by itself can translocate from the gut to pancreas and induce IDD, we inoculated only MF 13079 into germ-free adult C57BL/6 mice (Muri) by oral gavage. A mouse-derived strain, *Akkermansia muciniphila* 139, was inoculated into germ-free mice as control (Akk) [30]. Butyrate was not detected in either group (Fig. 5A), and the pancreatic *Cramp* gene expression level showed a trend of being lower in Muri group (Fig. 5B). MF 13079 attained a significantly higher load in the pancreas of Muri mice than *A. muciniphila* 139 in that of Akk mice (Fig. 5C), suggesting that the capacity of MF 13079 to translocate to the pancreas is much higher than that of *A. muciniphila* 139 in the case of mono-colonization. The Muri group, but not the Akk group, showed inflammation in the pancreas and development of IDD (Fig. 5D-F). Thus, MF 13079 alone can translocate from the gut to the pancreas, overgrew there and induce IDD.

To test whether MF 13079 can translocate from the gut to the pancreas and induce IDD when in competition with a complex normal gut microbiota and in a host with normal immunity, we transplanted cultured MF 13079 together with feces from control mice by oral gavage into antibiotic-treated mice ($FM_{NC+Muri}$). Antibiotic-treated mice inoculated with feces from control mice were denoted as FM_{NC}. We found that $FM_{NC+Muri}$ mice had significantly lower cecum butyrate levels and pancreatic *Cramp* expression than FM_{NC} mice (Fig. 6A and B). We obtained the absolute abundance of MF

(See figure on next page.)

Fig. 3 An increase in bacterial load and the impairment of immune tolerance in the pancreas. **A** Thirty ASVs that were significantly altered after 3 months of 0.2% DSS treatment, as identified using sPLS-DA models. The cluster tree on the left shows associations between these ASVs, as determined by the Spearman correlation coefficient based on their relative abundances among all the samples. The heat map shows the relative abundance (log_{10} transformed) of each ASV in a sample from an individual mouse. NC group, *n*=17; DSS group, *n*=18. **B** The butyrate content in the cecum of mice. NC, *n*=8; DSS, *n*=9; FM_{NC} *n*=8; FM_{DSS}, *n*=8. The bacterial load in the pancreas as measured by **C** real-time qPCR and **D** fluorescence in situ hybridization (FISH) of 16S rRNA. NC, *n*=8; DSS, *n*=9; FM_{NC}, *n*=5; FM_{DSS}, *n*=5. **E** Distribution of family-level phylotypes in the pancreas of NC and DSS-treated mice. The names of the top 10 most abundant families in the DSS group are shown. The abundance was determined by the relative abundances of these families with the total bacterial load in the pancreas detected with qPCR of 16S rRNA genes. NC, *n*=9; DSS, *n*=8. **F** The load of the 4 Muribaculaceae ASVs in the pancreas. The load was determined by multiplying the relative abundances of these ASVs with the total bacterial load in the pancreas detected with qPCR of 16S rRNA genes. NC, *n*=9; DSS, *n*=8. **G** *Cramp* expression in the pancreas of mice. NC, *n*=10; DSS, *n*=10; ABX_{NC}, *n*=6; ABX_{DSS}, *n*=6; FM_{NC}, *n*=5; FM_{DSS}, *n*=5. **H** Flow cytometry evaluation of leukocyte subtypes in the pancreas of NC and DSS-treated mice. Data are presented as the frequency of gated cells (from left to right: $F4/80^+$ macrophages, $CD3^+$ cells, $CD8^+$ T cells, $CD4^+$ T cells, and $Foxp3^+$ $CD4^+$ cells) among the $CD45^+$ population of cells per mouse. NC group, *n*=4-5; DSS group, *n*=4-5. The data are shown as the mean ± SEM, and Student's t-test (two-tailed) was used to analyze differences between the NC and DSS groups or the FM_{NC} and FM_{DSS} groups. **P* <0.05 and ***P* <0.01

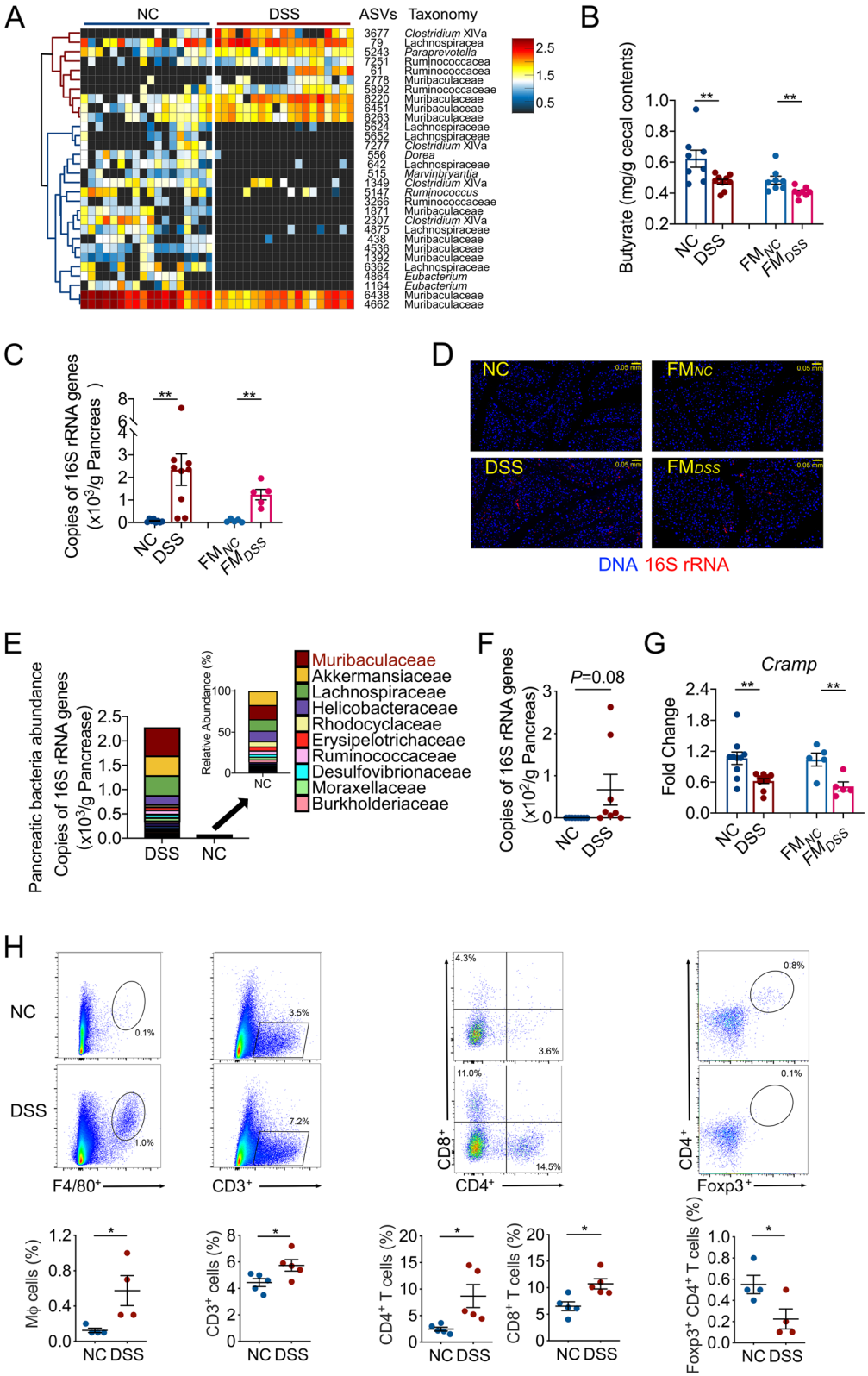

Fig. 3 (See legend on previous page.)

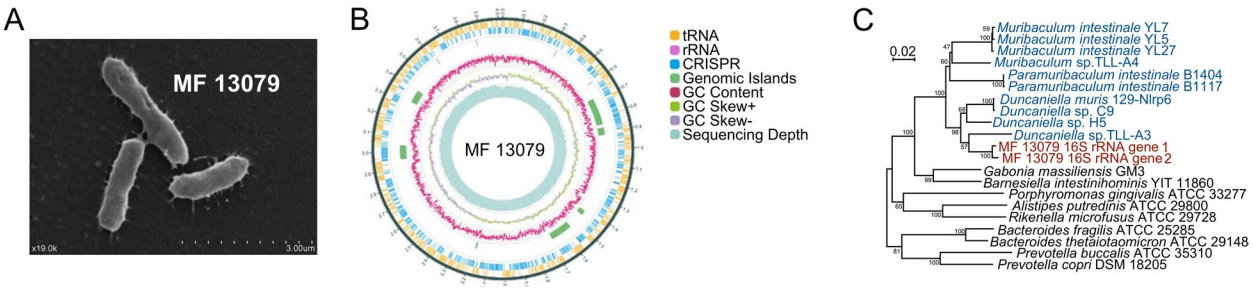

Fig. 4 A gut-derived Muribaculaceae isolate enriched by 0.2% DSS treatment **A** A scanning electron microscopy image of a pure isolate from the Muribaculaceae family (named strain MF 13079) that was enriched in the gut of DSS-treated mice. **B** Genome atlas of the MF13079 strain of Muribaculaceae. From outer to inner: circle 1. tRNAs; circle 2. rRNAs; circle 3. CRISPR sites; circle 4. mean centered GC content; circle 5. Sequencing depth. **C** A phylogenetic tree constructed with the 16 rRNA gene of MF 13079 (red), other Muribaculaceae bacteria (blue) and typical bacterial strains in Bacteroidota

13079 by multiplying the relative abundances of ASVs 6263 and 6451 with the total bacterial load in the pancreas detected with qPCR of 16S rRNA genes. We found that the load of MF 13079 in the pancreas of $FM_{NC+Muri}$ mice was three orders of magnitude higher than that in the pancreas of FM_{NC} mice (Fig. 6C). Concomitantly, the $FM_{NC+Muri}$ mice showed an inflammatory pancreatic milieu and increased blood glucose and decreased insulin in the OGTT (Fig. 6D-F). Thus, when transplanted together with the fecal microbiota from healthy mice, MF 13079 still translocated to pancreas and induced IDD in antibiotic-treated mice.

As recipient mice had normal gut barrier function, we tested other possible routes for translocation of gut pathobionts to pancreas. Notably, MF 13079 has a complete flagellar assembly pathway in its genome based on KEGG database querying, and a flagellar structure was observed with scanning electron microscopy (Fig. 4A, Figure S16 and Table S2). We tested bacterial motility by an agar-based motility assay, and MF 13079 demonstrated notable motility in vitro (Figure S15). It provides a means by which MF 13079 might translocate from the gut to the pancreas via the pancreatic duct. Interestingly, we also detected a much higher load of MF 13079 in the mesenteric lymph nodes of Muri mice than *A. muciniphila* 139 in those of Akk mice (Figure S17), which might represent another pathway for MF 13079 to gain access to the pancreas via lymphatic drainage routes [31, 32].

Dysbiotic gut microbiome from IDD patients including autoimmune T1D induced IDD in antibiotic-treated mice

To test whether the translocation of human-derived gut bacteria from IDD patients to the pancreas can induce the development of IDD in mice, we transplanted the fecal microbiota from 4 patients with IDD and 3 healthy participants to antibiotic-treated mice (denoted HFM_D and HFM_H, respectively). Among the four IDD patients, one was diagnosed to have the GADA antibody, confirmed as T1D, 2 showed no common T1D antibodies (GADA, IA-2A and ZnT8), one did not participate in antibody test. Each donor's fecal sample was inoculated into 6 antibiotic-treated mice. PCoA revealed that the population structure of the gut microbiota in the HFM_D mice was significantly different from that in HFM_H mice (P=0.001 by PERMANOVA test with 999 permutations) and that the gut microbiota of the recipient mice was more similar to that of the corresponding human donors (Figs. 7A and S18). Cecal butyrate content and pancreatic Cramp expression were significantly decreased in the HFM_D mice compared with the HFM_H mice (Fig. 7B and C). qPCR and FISH of 16S rRNA genes revealed that the total bacterial load in the pancreas of HFM_D mice was significantly higher than that in the pancreas of HFM_H mice (Figs. 7D-E and S19). Moreover, the HFM_D mice had an inflammatory pancreatic milieu, as shown by increased macrophage and total T cell population and decreased Treg cell populations compared with the HFM_H mice (Fig. 7F). Concomitantly, the HFM_D mice had significantly decreased insulin expression and number of islets in the pancreas, showed histological characteristics and phenotypes of mild pancreatitis (Fig. 7G-J), which may underlie the observed loss of insulin production and increased blood glucose levels. These results suggest that the gut microbiota from IDD patients has the capacity to translocate to the pancreas and induce the phenotypes of IDD in antibiotic-treated mice.

Discussion

Our study demonstrated that novel pathobionts enriched in a low DSS-disrupted gut microbiota can translocate to pancreas and induce IDD in mice. Such pathobionts are both necessary and sufficient to induce IDD. Genetic predisposition to IDD here was not required from the

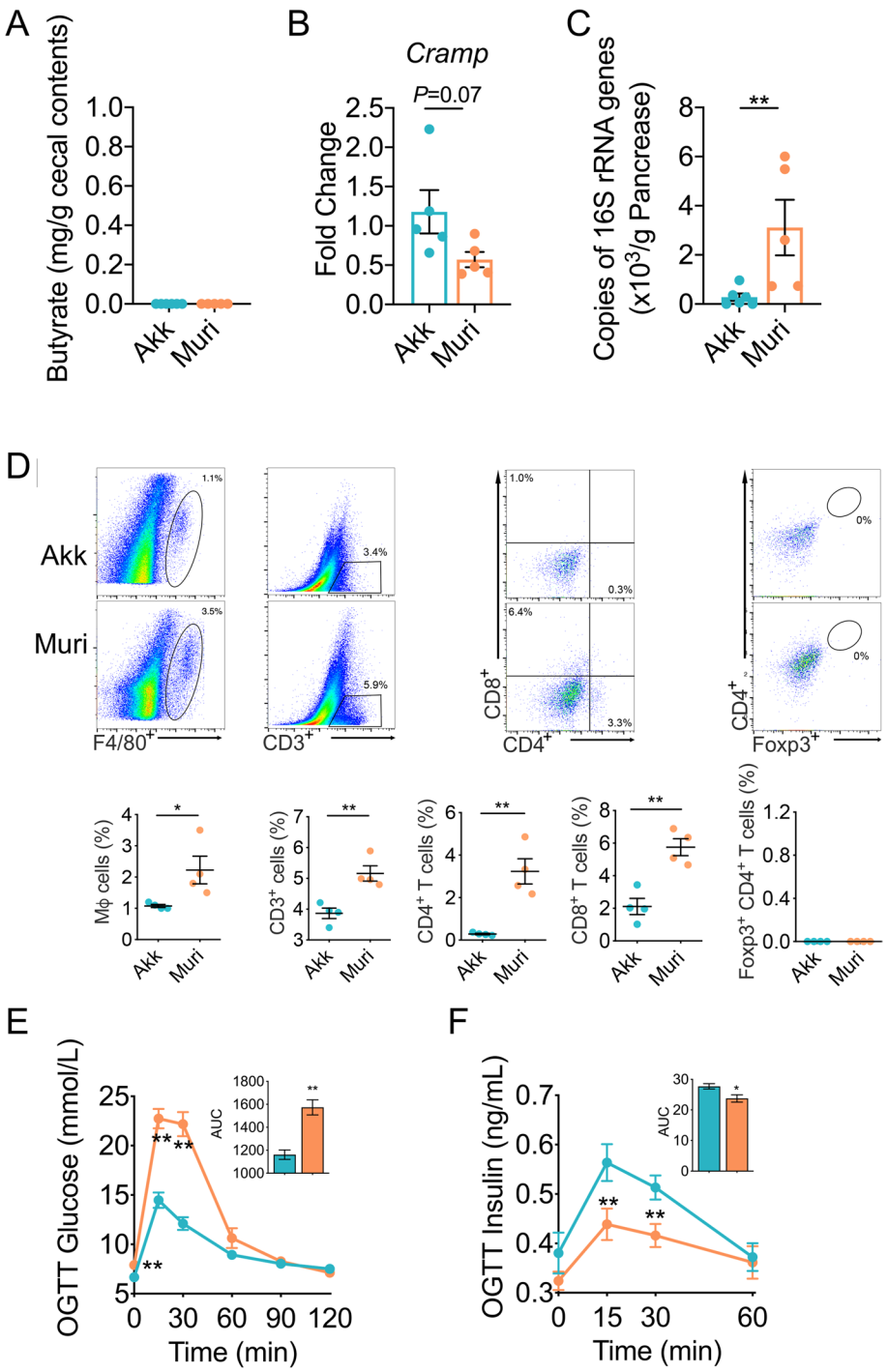

Fig. 5 MF13079 induced IDD by translocating to the pancreas in germ-free mice. **A** The butyrate content in the cecum of mice in the Muri and Akk groups. Akk, *n*=12; Muri, *n*=11. **B** *Cramp* expression in the pancreas of mice in the Muri and Akk groups. Akk, *n*=6; Muri, *n*=5. **C** The MF 13079 load in the pancreas of mice in the Muri and Akk groups assessed via qPCR of the 16S rRNA gene of each strain. Akk, *n*=6; Muri, *n*=5. **D** Flow cytometry evaluation of leukocyte subtypes in the pancreas of mice in the Muri and Akk groups. Data are presented as the frequency of gated cells (left to right: F4/80$^+$ macrophages, CD3$^+$ cells, CD8$^+$ T cells, CD4$^+$ T cells, and Foxp3$^+$ CD4$^+$ cells) among the CD45$^+$ population of cells per mouse. Akk, *n*=5; Muri, *n*=5. Blood glucose (**E**) and insulin (**F**) levels of the mice in Muri and Akk groups as measured by OGTT (the AUC is shown in the inset graph). For (**E**), Akk, *n*=12; Muri, *n*=11. For (**F**), Akk, *n*=10; Muri, *n*=10. Muri, germ-free mice inoculated with the MF 13079 strain and provided pure water; Akk, germ-free mice inoculated with the *Akkermansia muciniphila* strain 139 and provided pure water. In (**A**)-(**F**), the data are shown as the mean ± SEM, and Student's t-test (two-tailed) was used to analyze the differences between the Muri and Akk groups. **P* <0.05 and ***P* <0.01

host side as the mice we used were with no known relevant genetic defects. More importantly, a single isolated pathobiont MF 13079 corresponding to 2 of the 4 Muribaculaceae ASVs which were enriched in the gut and translocated to the pancreas in low DSS-treated mice, was sufficient to induce IDD when mono-associated with wildtype germfree mice. The fact that IDD was induced when MF 13079 was mixed with normal gut microbiota and transplanted to antibiotic treated wildtype mice which have well-developed immune system shows that predominant population level of this pathobiont in the gut is sufficient to IDD development. Thus, this pathobiont has been identified as an etiological factor for inducing IDD as what we did fulfilled Koch's postulates which were established for identifying the causal agent for an infectious disease.

Bacteria in the family Muribaculaceae (phylum Bacteroidota) are dominant in the gut microbiota of mice and generally detected in the intestine of other homeothermic animals [23, 33]. Due to the difficult isolation of this family, there are few studies on the biological functions of single strains of family Muribaculaceae. From the analysis of the draft genomes, the bacteria derived from the family Muribaculaceae may have abundant enzymes that decompose complicated carbohydrates and proteins, which help them adapt to environmental stress, such as changes of diets, and become the dominant bacteria in the gut [34, 35]. Not all the members of Muribaculaceae had the capacity for inducing IDD. Among the 4 ASVs, that were enriched by low DSS and translocated to pancreas, the genome of MF 13079 harbors 2. The other 2 ASVs may also have the capacity to induce IDD. This needs to be validated when we have their cultures. In previously published studies on microbiome and T1D, taxa other than Muribaculaceae were shown to be associated with T1D development in NOD mice [36]. There is a possibility that more pathobionts in different taxa may be found to have IDD inducing capacity. This IDD-inducing capacity may be a redundant function of many gut pathobionts in the same mouse, however, translocation of one such pathobiont to pancreas seems to be enough for inducing IDD and host genetic defect is not required.

Studies in humans have shown that acute or chronic inflammation of the entire pancreas may drive beta-cell death and lead to IDD [37]. Translocation of pathobionts to pancreas has been shown a pivotal role in inducing various pancreatic diseases [25]. A previous study showed that the deficiency of butyrate in NOD mice induced decreased production of CRAMP by pancreatic β-cell, which has been linked with the development of autoimmunity in pancreas and type 1 diabetes, but the mechanism is unclear [16]. Pancreatic CRAMP can change the gut microbiota and intestinal immunity when secreted to the gut via the pancreatic duct, but its relationship with pancreatic microbiome is not known [38]. Our study showed that enrichment and overgrowth of pathobionts in the pancreas is necessary for CRAMP-induced stimulation of local immune cells because antibiotic removal of the gut microbiota resulted in pancreatic microbiome depletion and abolished DSS-induced IDD.

Intriguingly, the dysbiotic gut microbiota from IDD patients including autoimmune T1D also induced IDD in antibiotic-treated wildtype mice. This indicates that IDD-inducing pathobionts may exist in the gut microbiota of these patients. Genetic predisposition is known to play an important role in T1D development, but the mechanism involved remain elusive. One possibility could be that the genetic defect leads to disruption of the gut microbiota with enrichment of pathobionts which translocate to pancreas and induce IDD. Our study provides strong evidence to support this hypothesis. The result that the dysbiotic gut microbiota from IDD patients was sufficient to induce IDD in antibiotic-treated mice indicates that we may be able to identify and isolate IDD-inducing pathobionts from the patients' gut microbiota following the strategy established in this study.

Studies showed that reduced butyrate production in the gut may drive the decreased gene expression of pancreatic CRAMP [16]. This might be a mechanism for induction of pancreatic inflammation and IDD in our low DSS model. The low dose DSS treated mice had depletion of butyrate producers and reduced butyrate production in their gut and decreased gene expression of pancreatic CRAMP. This warrants further studies.

(See figure on next page.)

Fig. 6 MF 13079 translocated from the gut to the pancreas and induce IDD when in competition with a complex gut microbiota. **A** The butyrate content in the cecum of FM_{NC} and $FM_{NC+Muri}$ mice. FM_{NC}, n=10; $FM_{NC+Muri}$, n=10. **B** *Cramp* expression in the pancreas of FM_{NC} and $FM_{NC+Muri}$ mice. FM_{NC}, n=5; $FM_{NC+Muri}$, n=5. **C** The amount of the MF 13079 in the pancreas of $FM_{NC+Muri}$ and FM_{NC} mice assessed with the method described in Fig. 3F. FM_{NC}, n=4; $FM_{NC+Muri}$, n=5. **D** Flow cytometry evaluation of leukocyte subtypes in the pancreas of $FM_{NC+Muri}$ and FM_{NC} mice. Data are presented as the frequency of gated cells (left to right: F4/80$^+$ macrophages, CD3$^+$ cells, CD8$^+$ T cells, CD4$^+$ T cells, and Foxp3$^+$ CD4$^+$ cells) among the CD45$^+$ population of cells per mouse. FM_{NC}, n=4; $FM_{NC+Muri}$, n=4. Blood glucose (**E**) and insulin (**F**) levels of $FM_{NC+Muri}$ and FM_{NC} mice as measured by an OGTT (the AUC is shown in the inset graph). For (**E**), FM_{NC}, n=10; $FM_{NC+Muri}$, n=10. For (**F**), FM_{NC}, n=8; $FM_{NC+Muri}$, n=10. FM_{DSS}, antibiotic cocktail-treated mice inoculated with the fecal microbiota from mice in the DSS group and provided pure water; $FM_{NC+Muri}$, antibiotic cocktail-treated mice inoculated with a mixture of the fecal microbiota of the NC group and the MF 13079 strain and provided pure water. In (**A**)-(**F**), the data are shown as the mean ± SEM, and Student's t-test (two-tailed) was used to analyze the differences between the FM_{NC} and $FM_{NC+Muri}$ groups. *P <0.05 and **P <0.01

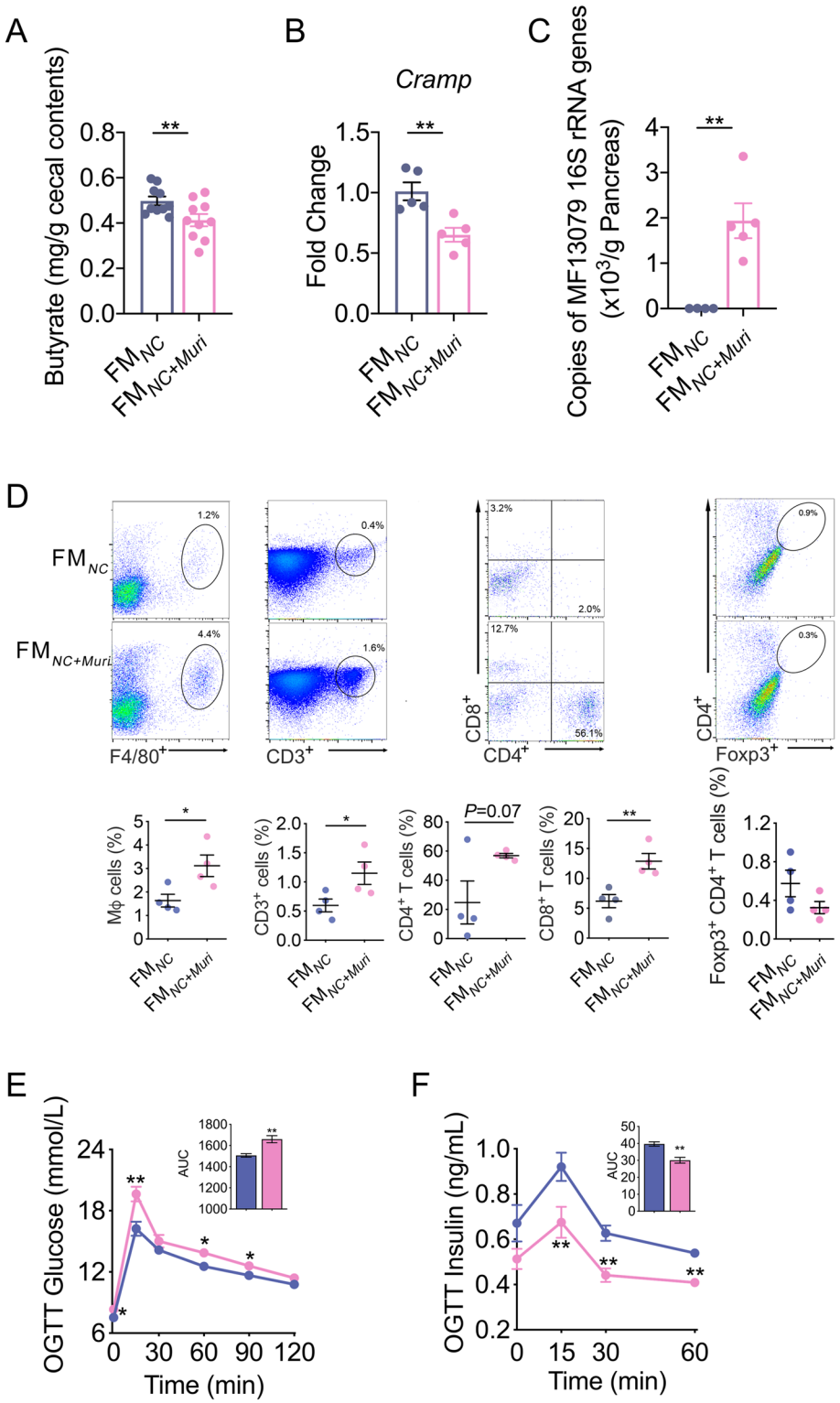

Fig. 6 (See legend on previous page.)

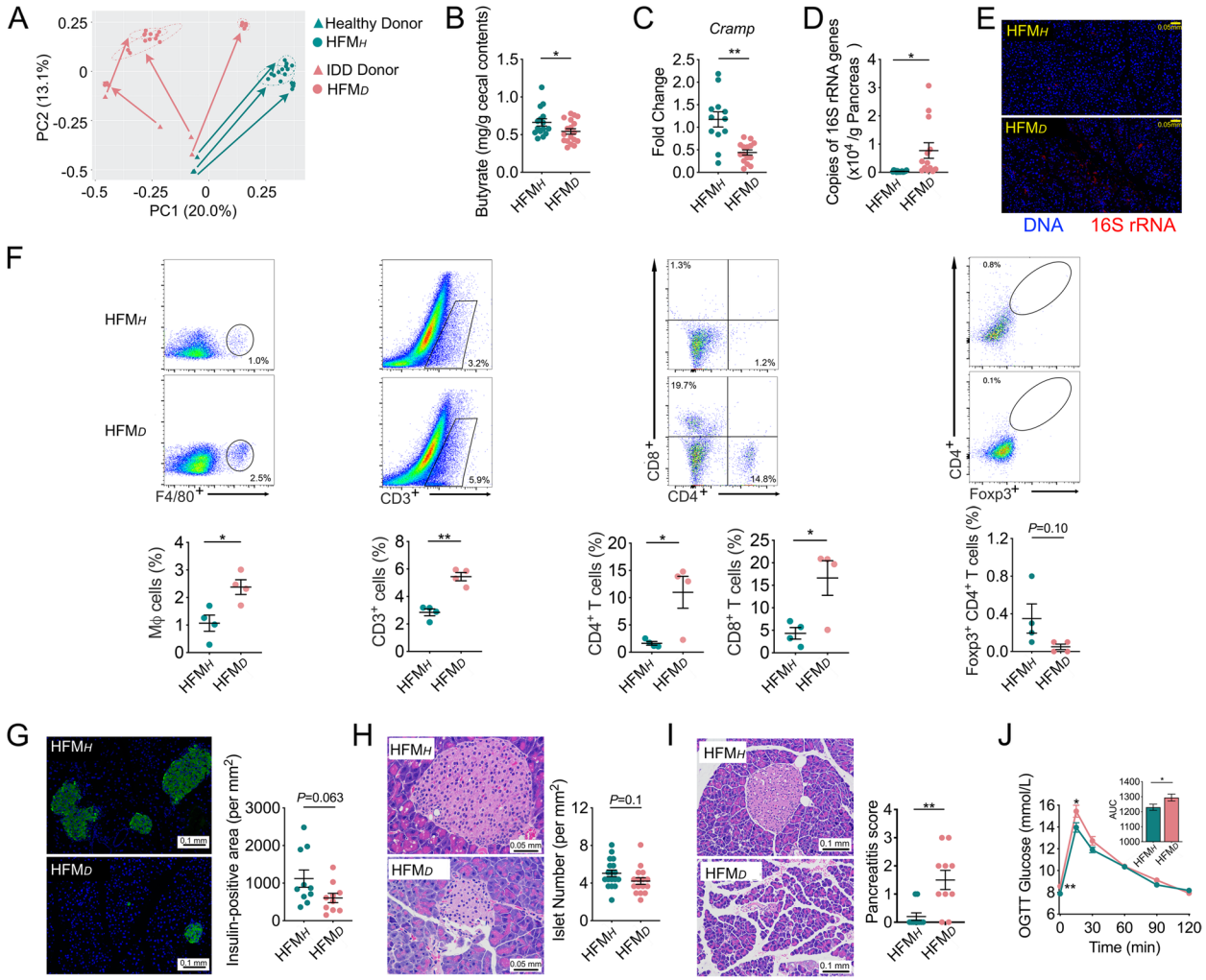

Fig. 7 The gut microbiota from patients with IDD increased the bacterial load in the pancreas, disrupted local immune tolerance and induced IDD in recipient mice. **A** The overall structure of the gut microbiota of the IDD patients, healthy human donors, and mouse recipients. Principal coordinate analysis (PCoA) was performed on the basis of Bray-Curtis distance at the amplicon sequence variant (ASV) level. The bacterial load in the pancreas of HFM_H and HFM_D mice as measured by **B** real-time qPCR and **C** FISH of 16S rRNA genes. HFM_H, n=16; HFM_D, n=13. **D** Flow cytometry evaluation of leukocyte subtypes in the pancreas of mice in the HFM_H and HFM_D groups. Data are presented as the frequency of gated cells (left to right: F4/80$^+$ macrophages, CD3$^+$ cells, CD8$^+$ T cells, CD4$^+$ T cells, and Foxp3$^+$ CD4$^+$ cells) among the CD45$^+$ population of cells per mouse. HFM_H, n=4; HFM_D, n=4. **E** Histological sections of pancreatic tissue (scale bar = 0.1 mm) from HFM_H and HFM_D mice stained for insulin (green) and DNA (blue). The insulin-positive area in pancreatic tissue was calculated. HFM_H, n=10; HFM_D, n=10. **F** H&E-stained histological sections of pancreatic tissue (400x, scale bar = 0.05 mm) from HFM_D mice and HFM_H mice. The number of islets per mm2 of pancreatic tissue was counted. HFM_H, n=18; HFM_D, n=16. **G** H&E-stained histological sections of pancreatic tissue (200x, scale bar = 0.1 mm) from HFM_H and HFM_D mice. The histologic pancreatitis score was evaluated by edema, inflammation, and vacuolization. HFM_H, n=10; HFM_D, n=10. **H** The blood glucose level of HFM_H and HFM_D mice according to OGTT (the AUC is shown in the inset graph). HFM_H, n=4; HFM_D, n=4. HFM_H, antibiotic cocktail-treated mice inoculated with the fecal microbiota of healthy human donors; HFM_D, antibiotic cocktail-treated mice inoculated with the fecal microbiota of IDD patients. The data are shown as the mean ± SEM, and Student's t-test (two-tailed) was used to analyze differences between groups. *P <0.05 and **P <0.01

Conclusion

Our study shows that toxic chemicals such as DSS may disrupt the gut microbiota and lead to serious health consequences even at a low dosage which does not cause acute local responses in the gut. The overgrowth in the gut and translocation to the pancreas of pathobionts may induce inflammation in the pancreas, destruct beta cells and lead to IDD. This study inspires us to search for similar pathobionts in patients with IDD. Suppression of the overgrowth of pathobionts in the gut and prevention of their translocation to the pancreas via restoration of a normal structure of the gut microbiota may become a promising ecological approach for managing IDD.

Methods

Animal trials

Mice

Five-week-old SPF male mice (C57BL/6) were obtained from SLAC Inc. (Shanghai, China) and kept under SPF environment at the animal facility of Shanghai Jiao Tong University, Shanghai, China. Mice (three-five mice/cage) were housed in IVC system cages (Dimensions 325 × 210 × 180 mm; Suzhou Fengshi Laboratory Animal Equipment Co., Ltd). The mice were fed with a sterilized normal chow diet (10% energy from fat; 3.25 kcal/g; 1010009, SLAC) and were housed in a room maintained at 22.0 ± 1°C with 30-70% humidity, with a 12 h light/dark phase cycle (lights on at 07:00 am).

Eight-week-old of germ-free male C57BL/6 mice were maintained in flexible-film plastic isolators at the Laboratory Animal Center of the SLAC Inc. (Shanghai, China). The mice were fed a sterilized normal chow diet (10% energy from fat; 3.25 kcal/g; P1103F-50, SLAC). The mice were housed in a room maintained at 22.0 ± 1°C with 30-70% humidity with a 12 h light/dark phase cycle (lights on at 06:00 am). Surveillance for bacterial contamination was performed by periodic bacteriological examinations of feces, food and padding. Detailed operations of surveillance for bacterial contamination were consistent with previous work [39].

Animal trials

Trial-1 After one-week of acclimation, the mice were randomly assigned to 2 groups: (i) NC group (n = 7-10), control mice provided pure drinking water for feeding 12 weeks; (ii) DSS group (n = 7-10), mice treated with 0.2% (w/v) DSS (0216011080, MP Biomedicals, USA) to drinking water for feeding 12 weeks. Independently repeated trials were performed three times.

Trial-2 After one-week of acclimation, a cocktail of antibiotics (0.5 g/L of vancomycin, 1 g/L of ampicillin, 1 g/L of neomycin, 1 g/L of metronidazole) was introduced in drinking water [40]. For 5 weeks. The mice were then randomly assigned to 2 groups: (i) ABX_{NC} group (n = 10), antibiotic cocktail-treated mice provided pure drinking water for 12 weeks; (ii) ABX_{DSS} group (n = 8), antibiotic cocktail-treated mice with 0.2% (w/v) DSS added to drinking water for 12 weeks. During the 12 weeks, both groups continued to have the antibiotic cocktail in their drinking water.

Trial-3 After one-week of acclimation, the antibiotic cocktail was introduced in drinking water for 5 weeks. The mice were then randomly assigned to 2 groups: (i) FM_{NC} group (n = 10), antibiotic cocktail-treated mice inoculated with the fecal inoculum from mice in the NC group and provided pure water for feeding 20 days; (ii) FM_{DSS} group (n = 10), antibiotic cocktail-treated mice inoculated with the fecal inoculum from mice in the DSS group and provided pure water for feeding 20 days. The oral gavage was performed once a day for 3 times (Day 0, Day 1 and Day 4). Each mouse was given 200 μL of inoculum every time.

Trial-4 After one-week of acclimation, the antibiotic cocktail was introduced in drinking water for 5 weeks. The mice were then randomly assigned to 2 groups: (i) FM_{NC} group (n = 10), antibiotic cocktail-treated mice inoculated with the fecal inoculum from mice in the NC group and provided pure drinking water for 20 days; (ii) $FM_{NC+Muri}$ group (n = 10), antibiotic cocktail-treated mice inoculated with a mixture of the fecal inoculum of the NC group and the MF 13079 strain and provided pure drinking water for 20 days. The oral gavage was performed once a day for 3 times (Day 0, Day 1 and Day 4). Each mouse was given 200 μL of fecal inoculum every time in FM_{NC} group; and each mouse was given 100 μL fecal inoculum and 100 μL bacterial suspension in $FM_{NC+Muri}$ group.

Trial-5 The germ-free mice were randomly assigned to two groups and each group was kept in an individual plastic isolator. (i) Akk group (n = 12), germ-free mice inoculated with the *Akkermansia muciniphila* strain 139 and provided pure drinking water for 14 days; (ii) Muri group (n = 11), germ-free mice inoculated with the MF 13079 strain and provided pure drinking water for 14 days. The oral gavage was performed once a day for 2 consecutive days. Each mouse was given 200 μL of bacterial suspension every time.

Trial-6 After one-week of acclimation, an antibiotics cocktail was introduced in drinking water. After 5 weeks, the mice were randomly assigned to 2 groups: (i) HFM_{H} group (n = 18), the mice were inoculated with fecal inoculum from healthy human donors (n = 3) by oral gavage and maintained for 20 days; (ii) HFM_{T1DM} group (n = 24), the mice were inoculated with fecal inoculum from IDD patients (n = 4) by oral gavage and maintained for 20 days. Fecal sample from each volunteer was prepared separately and 6 mice were inoculated with each inoculum. The oral gavage was performed once a day for 3 times (Day 0, Day 1 and Day 4). Each mouse was given 200 μL of inoculum every time.

Sequence-guided bacteria isolation

Fresh fecal samples from DSS group were collected and mixed in anaerobic sterile Ringer working buffer in an

anaerobic workstation (Don Whitley Scientific Ltd, Shipley, UK). The 10^5 diluted suspension with Ringer working buffer was placed onto 46 medium plates (Table S1) and incubated under anaerobic condition (80% N_2, 10% CO_2, and 10% H_2) at 37°C for 7 days. The 16S rRNA gene of each colony was obtained using the primers 27-F (AGAGTTTGATCCTGGCTCAG) and 1492-R (GGTTACCTTGTTACGACTT). The obtained 16S rRNA sequences were sequenced and aligned with the ASVs in Muribaculaceae enriched in the gut of DSS-treated mice. One Muribaculaceae strain (MF13079) was isolated using a previously reported MPYG medium [41] which was modified by adding 3% fetal bovine serum (FBS, GIBCO, 10099-141). The Muribaculaceae strain MF13079 16S rRNA sequence was aligned with the GenBank. All the 16S rRNA sequence of the isolated strains in the family Muribaculaceae and the 16S rRNA sequence of the representative strains in other families of the phylum Bacteroidota were selected to build a phylogenetic tree by using the Neighbor-Joining method in MEGA 6.

Preparation of inoculum

Preparation of inoculum from mice feces

Fresh fecal samples from each mouse in NC and DSS groups (in the 12th week of Trial-1) were collected. The fecal samples in the same group were mixed in anaerobic sterile Ringer working buffer (9 g/L of sodium chloride, 0.4 g/L of potassium chloride, 0.25 g/L of calcium chloride dehydrate and 0.05% (w/v) L-cysteine hydrochloride) in an anaerobic chamber (80% N_2 :10% CO_2 :10% H_2) [42], and diluted to 50 times. Then the suspensions were added with 20% (w/v) skim milk (LP0031, Oxoid, UK) and the final fecal suspensions were diluted to 100 times. The fecal suspensions were preserved at − 80 °C until inoculation.

Preparation of inoculum from human feces

Recruitment of volunteers was approved by the ethics committee of Henan Provincial People's Hospital and all participants gave written informed consent (registration number: ChiCTR2000030049). Four IDD patients and three age- and sex-matched healthy controls were recruited. Diabetes diagnosis was performed according to the 1999 World Health Organization criteria [43]. IDD was diagnosed following criteria: acute-onset ketosis or ketoacidosis with immediate insulin replacement therapy; impaired islet function. Among the four IDD patients, one was diagnosed to have the GADA antibody, confirmed as classical T1D, 2 showed no common T1D antibodies (GADA, IA-2A and ZnT8), one did not participate in antibody test. All healthy controls were negative for GADA, IA-2A and ZnT8A.

Preparation of bacterial suspensions

Akkermansia muciniphila strain 139 was cultured in a synthetic medium [44] and Muribaculaceae strain MF13079 was cultured in a modified MPYG medium (Table S1). The harvested bacterial cells were washed twice with PBS (pH 7.4) and resuspended in PBS (pH 7.4) and added with equal volume of 20% skim milk to a density of 10^9 cells/ml. The bacterial suspensions were stored at − 80 °C until inoculation.

Glucose tolerance test and estimation of insulin sensitivity

Oral glucose tolerance test (OGTT)

The first batch of mice were fasted for 6 h and baseline blood glucose levels were measured with an Accu-Check Performa blood glucose meter (Roche, USA) using blood collected from the tail vein. After administration of glucose (2.0 g/kg body weight) via oral gavage, blood glucose levels were measured at 15, 30, 60, and 120 min. Serum insulin levels were also measured by ELISA kit (90080, Crystal Chem, USA) at 0, 15, 30, 60 min after glucose challenge.

Insulin tolerance test (ITT)

Six hours fasted second batch of mice were injected intraperitoneally with 1.0 U insulin/kg body weight (Novolin, Novo Alle, Denmark). Blood glucose was then measured at 0, 15, 30, 60, and 120 min after injection with the blood glucose meter (Roche, USA).

In vivo intestinal permeability assay

Intestinal permeability was measured based on the permeability to 4000 Da-FITC-dextran in plasma (DX-4000-FITC) (46944; Sigma-Aldrich, St. Louis, Missouri, USA) as previously described [45]. Briefly, after fasting for 6 h, the mice were administered with DX-4000-FITC (500 mg/kg body weight, 125 mg/mL) by oral gavage. After 4 h, blood plasma collected from the tip of the tail vein was diluted with equal volume of PBS (pH 7.4) and analyzed for DX-4000-FITC concentration with a fluorescence spectrophotometer (HTS-7000 Plus-plate-reader; Perkin Elmer, Wellesley, Massachusetts, USA) at an excitation wavelength of 485 nm and emission wavelength of 535 nm. A standard curve was obtained by diluting FITC-dextran in non-treated plasma diluted with PBS (1:3 v/v).

Energy assessment of feces

Fecal output measurement

Mice were placed in a clean cage individually and feces were collected for 24 h. Dry weights were taken after fecal pellets were incubated at 65°C in an oven for 24 h (JC101, Shanghai Chengshun Instrument & Meter Co., Ltd, Shanghai, China).

Bomb calorimetry

Bomb calorimetry was performed on dried fecal pellets. Gross energy content was measured using an isoperibol bomb calorimeter (C6000, IKA, Germany). The calorimeter energy equivalent factor was determined using benzoic acid standards.

Triglycerides and cholesterol measurement

Serum cholesterol and triglycerides were quantified with colorimetric kits (A111-1-1-1 and A110-1-1, respectively) from Nanjing Jiancheng Bioengineering Institute (Nanjing, China).

Frozen liver sample was homogenized in a corresponding volume (1:9, w:v) of homogenizing buffer (pH 7.4, 0.01 mol/L Tris-HCl, 0.1 mmol/L EDTA-2Na, 0.8% NaCl). The supernatant was collected after centrifugation for 25 min at 2,000×*g* and 4 °C. Cholesterol and triglycerides in homogenized tissue were quantified by colorimetric kits from Nanjing Jiancheng Bioengineering Institute (Nanjing, China). Tissue homogenized total protein was measured with the Protein Quantification Kit (20202ES76; Yeasen Biotechnology Ltd., Shanghai, China).

Amylase and lipase measurement

Serum amylase and lipase were quantified with colorimetric kits (C016-1-1 and A054-2-1, respectively) from Nanjing Jiancheng Bioengineering Institute (Nanjing, China).

Fecal lipocalin-2 detection

Fecal lipocalin-2 content was quantified with a Lipocalin-2/NGAL Quantikine ELISA kit (DLCN20, R&D Systems).

mRNA expression of genes related with gut barrier integrity in the colon

The total RNA of colons was extracted using the RNeasy Plus Universal Tissue Mini Kit (73404, Qiagen, Duesseldorf, Germany). The RNA was reverse-transcribed to cDNA using the SuperScript™ III First-Strand Synthesis (18080051, Invitrogen, Calif., USA). RT-qPCR was performed with the Light Cycler 96 (Roche, Geneva, Switzerland) using iQ SYBR Green Supermix (170-8882AP, BIO-RAD, CA, USA). The PCR conditions were 95°C for 3 min, followed by 40 cycles of 95°C for 20 s, 56°C for 30 s, and 72°C for 30 s, and plate reads for 5 s. Gene expression levels were determined using the comparative $\Delta\Delta C_T$ method ($2^{-\Delta\Delta C}{}_T$ method), with the β-actin gene serving as the housekeeping gene. Forward (F) and reverse (R) primer sequences are as follows:

β-actin, F-CCTTCTTGGGTATGGAATCCTGTG, and R-CAGCACTGTGTTGGCATAGAGG;
*Tjp*1, F-ACCCGAAACTGATGCTGTGGATAG, and R-AAATGGCCGGGCAGAACTTGTGTA;
*Cldn*1, F-GATGTGGATGGCTGTCATTG, and R-CCTGGCCAAATTCATACCTG;
*Muc*1, F-TACCCTACCTACCACACTCACG, and R-CTGCTACTGCCATTACCTGC;
*Muc*2, F-CACCAACACGTCAAAAATCG, and R-GGTCTCTCGATCACCACCAT;
*Muc*3, F-CTTCCAGCCTTCCCTAAACC, and R-TCCACAGATCCATGCAAAAC;
*Muc*4, F-GAGAGTTCCCTGGCTGTGTC, and R-GGACATGGGTGTCTGTGTTG;
Zo-1, F-ACCCGAAACTGATGCTGTGGATAG, and R-AAATGGCCGGGCAGAACTTGTGTA;
Occludin, F- ATGTCCGGCCGATGCTCTC, and R-TTTGGCTGCTCTTGGGTCTGTAT.

Histopathology

Fresh epididymal fat pads were fixed with 4% paraformaldehyde for 48 h, embedded in paraffin, sectioned, and stained with hematoxylin and eosin (H&E) (G1003; Wuhan Servicebio technology Ltd., Wuhan, China). Digital images of sections were acquired with a Leica DMRBE microscope. Adipocyte sizes were assessed using Image Pro Plus v6.0 (Media Cybernetics Inc., Silver Springs, MD, USA). For each mouse, mean areas of adipocytes were determined in five discontinuous scans under ×200 magnification.

Fresh liver tissues were fixed with 4% paraformaldehyde for 48 h, embedded in paraffin, sectioned, and stained with hematoxylin and eosin (H&E) (G1003; Wuhan Servicebio technology Ltd., Wuhan, China). Digital images of sections were acquired with a Leica DMRBE microscope. For Oil Red O staining of liver sections, liver tissues were fixed in 4% paraformaldehyde for at least 48 h, embedded in optimal cutting temperature (OCT) compound (4583; CellPath Ltd., Newtown, Powys, UK) and frozen at −20 °C. Sections were stained with Oil Red O (O0625; Sigma-Aldrich Ltd., St. Louis, MO, USA). Digital images of sections were acquired with a Leica DMRBE microscope.

Fresh pancreatic tissues were fixed with 4% paraformaldehyde for 48 h, embedded in paraffin, sectioned, and stained with hematoxylin and eosin (H&E) (G1003; Wuhan Servicebio technology Ltd., Wuhan, China). Digital images of sections were acquired with a Leica DMRBE microscope. pancreas islet number were assessed using Image Pro Plus v6.0 (Media Cybernetics Inc., Silver Springs, MD, USA). Histological analysis of pancreatitis

was determined by one observer who was blinded to the treatment group. Scores of pancreatitis severity was assessed as described previously [46].

Immunofluorescence observation of insulin in the pancreas

Fresh pancreatic tissues were fixed with 4% paraformaldehyde and then embedded in paraffin. Subsequently, 4 μm sections were blocked with 5% bovine albumin (BSA), and stained overnight with anti-insulin pAb (1:500, Abcam, ab7842) at 4°C. After washing, anti-pig-AlexaFluor488 secondary antibody as the second-step reagents were applied. The sections were incubated for 15 min at room temperature in the dark. Nuclei were stained with DAPI (G1012, Servicebio). Digital images of sections were acquired with a Leica DMRBE microscope after completely rinsing with sterile PBS. The insulin-positive area of each section was counted with the 'automatic bright objects' option in the 'Measure/count/size' panel in Image Pro Plus v6.0 (Media Cybernetics Inc., Silver Springs, MD, USA).

Immunohistochemical analysis of ZO-1 and occludin in the colon

After deparaffinization and processing for antigen retrieval, the blank colon sections were incubated overnight at room temperature with anti-rabbit ZO-1 antibody (1:500, catalog no. GB11195; Servicebio, China) and Occludin antibody (1:200, catalog no. GB11149; Servicebio) separately. Sections were then incubated with anti-rabbit IgG secondary antibody (KPL, MA, USA) for 50 min at room temperature. After washing with PBS, the DAB Envision kit (catalog no. K5007; Dako, Copenhagen, Denmark) was used to develop color; ZO-1 and Occludin appear brown, while nuclei are blue. Images of each colon section were obtained in tripartite by experienced staff who were blind to the experiment under ×200 magnification using a Leica DMRBE microscope and were analyzed using Image Pro Plus 6.0, according to the method previously described [47]. The integrated optical density (IOD) values were log10 transformed.

Flow cytometry evaluation of subtypes of leukocytes in the pancreas

Randomly selected 2-3 mice in the NC group and DSS group of each batch of animals were harvested fresh pancreatic samples for flow cytometry. Fresh pre-cut pancreatic tissue (2 × 2 mm) were digested with a solution of collagenase P in HBSS-1% HEPES (0.75 mg/mL, Roche) at 37°C for 7 min with shaking. Digestion was stopped by adding HBSS-10% FCS 1% EDTA followed by extensive washes by FACS buffer (1×PBS pH7.2, 0.5% BSA, 2mM EDTA). The suspensions were filtered through 100 μm cell strainer (352360, FALCON, USA). Suspensions were transfer into Polystyrene Round-Bottom Tube (352052, FALCON, USA) followed by centrifugation at 400×g at 4°C for 5 min. To ensure single cell bioactivity, it was necessary to disperse the cells quickly after discarding the supernatant. 500 μL FACS buffer was added to re-suspend cells. The wash step was repeated twice to get a single cell suspension. Non-specific binding was blocked with FcR blocking antibody (anti-mouse CD16/32, 553142, BD Pharmingen) before surface staining with the following mAbs: Anti-mouse CD45.2 (563051, BD Horizon), Anti-mouse-CD3e (562600, BD Horizon), Anti-mouse-CD4 (553653, BD Pharmingen), Anti-mouse-CD8a (551162, BD Pharmingen), Anti-mouse-F4/80 (12-4801-82, eBioscience). Single cell suspension was washed twice as described above by 500 μL FACS buffer. Intracellular staining was carried out after fixation and permeabilization (00-5523-00, eBioscience) with the following antibodies: Anti-mouse Foxp3 (77-5775-40, eBioscience). Dead cells were excluded with a fixable viability dye (65-086514, Invitrogen, USA). The fluorescence was examined on an Flowcytometer (BD LSRFortessa, Becton, Dickinson and Company, USA).

Short-chain fatty acids (SCFAs) profiling

For the determination of SCFAs in cecum content, 200 mg cecum content was homogenized with 1 mL PBS (pH=7.2) and centrifuged at 16000 × *g* for 15 min (4°C). The supernatants were filtered through 0.22 μm filters. 100 μL of cecal content water sample was acidified by adding 0.1 mL of 50% (v/v) sulfuric acid. After vortexing and standing for 2 min, the organic acids were extracted by adding 0.4 mL of diethyl ether. Then the concentration of SCFAs was measured using the Agilent 6890 (Agilent Technologies, CA, USA) with flame ionization, thermal conductivity detectors, and capillary column.

Whole-genome sequencing and analysis of MF13079

Whole-genome DNA of Muribaculaceae strain MF13079 was extracted with QIAamp BiOstic Bacteremia DNA Kit (12240-50, Qiagen, USA) and sequenced with the Oxford@ Nanopore PromethION platform (performed by Nextomics Biosciences, Wuhan, China). Subreads of the sequence were assembled into a single complete chromosome using the HGAP 2.3.0 pipeline [48].

The genome sequence of Muribaculaceae strain MF13079 was adjusted to start with the replicational origin (location of *DnaA*) for comparison. Protein-coding sequences (CDSs), tRNAs, and rRNAs were predicted and annotated using the Prokka 1.12 pipeline (Table S2) [49]. Functional annotation of genes related with flagella-synthesis in the CDSs of MF13079 was performed using

the Kyoto Encyclopedia of Genes and Genomes (KEGG) database.

Microbiota profiling in tissues

DNA extraction of microorganisms in tissues

Pre-cut pancreatic tissue (5 × 5 mm) and mesenteric lymphatic nodes (MLNs) were homogenized using a sterile pestle in a sterile mortar under liquid nitrogen as the media. Homogenate was used for DNA extraction by QIAamp Pro DNA Kit (51804, Qiagen, Duesseldorf, Germany). Sterile DNA-free water was used as negative controls.

Bacterial load in the pancreas and mesenteric lymphatic nodes (MLNs)

Nested PCR was used in this situation. The 16S rRNA gene was first amplified using the primers 27-F (AGAGTTTGATCCTGGCTCAG) and 1492-R (GGTTACCTTGTTACGACTT). PCR was performed in a volume of 25.0 µl with 10 ng DNA template, 1 µl of each primer (12.5 µM), 2.5 µl of 10× PCR buffer, 0.3 µl of Taq polymerase (TaKaRa), 1 µl of dNTP mix (2.5 mM). The reaction conditions consisted of initial denaturation at 94 °C for 5 min; 25 cycles of 94 °C for 30 s, 55 °C for 30 s and 72 °C for 90 s; and a final extension step for 10 min at 72 °C. Subsequently, a 466 bp length sequence located in 16S rRNA gene was used for quantitative PCR through the primers Uni331F (TCCTACGGGAGGCAGCAGT) and Uni797R (GGACTACCAGGGTATCTAATCCTGTT) [50]. Briefly, qPCR was performed with the Light Cycler 96 (Roche, Geneva, Switzerland) using iQ SYBR Green Supermix (170-8882AP, BIO-RAD, CA, USA). The PCR conditions were 95°C for 3 min, followed by 40 cycles of 95°C for 15 s, 60°C for 60 s and plate read for 5 s at 80°C. A whole-length 16S rRNA gene of an *Akkermansia muciniphila* strain derived from mice intestine was used to plot a standard curve to calculate the copies of 16S rRNA genes in the samples.

Fluorescence in situ hybridization (FISH) of 16S rRNA in the pancreas

The EUB338 16S rRNA probe labeled with the fluorophore Cy3 (extinction wavelength, 555 nm; emission wavelength, 570 nm; Servicebio, China) was used to detect the bacterial colonization within mouse pancreatic tissues by FISH. Nuclei were stained with DAPI (G1012, Servicebio). Fluorescence microscopic analysis was conducted with Nikon Eclipse 90i confocal microscope (Nikon, Melville, NY) using a Cy3 labeled-probe at 1µM as described [51–53].

Pancreatic microbiota analysis by sequencing of V3-V4 region in 16S rRNA gene

The 16S rRNA gene was first amplified from total DNA of the second batch of pancreatic tissue using the primers 27-F (AGAGTTTGATCCTGGCTCAG) and 1492-R (GGTTACCTTGTTACGACTT). The PCR products were used as a template, a sequencing library of the V3-V4 region of the 16S rRNA gene was constructed following the manufacturer's instructions (Part # 15044223Rev.B; Illumina Inc., San Diego, CA, USA) with improvement as previously described [20], and sequenced on the Illumina MiSeq platform (Illumina, Inc., San Diego, CA, USA). The negative controls from DNA extraction step were amplified and sequenced. Sterile DNA-free water was also used as template for PCR in sequencing library preparation and then sequenced.

The raw paired-end reads were processed and analyzed using the Quantitative Insights into Microbial Ecology 2 (QIIME2, v2019.01) platform [41]. Demultiplexed sequence data was imported into QIIME2, adapters and primers were trimmed. Amplicon sequence variants (ASVs) from each sample was inferred by using the DADA2 pipeline [54] for filtering, dereplication, sample inference, merging of paired-end reads and chimera identification. In the process of running the DADA2 pipeline, based on the quality profile of the data, forward and reverse reads were trimmed accordingly to ensure that the median quality score for each position is above 32. Potential reagent and environmental contaminations were identified using "decontam (v.1.2.1)" package in R (v3.4.4) based on the frequency of the ASV in the negative controls with threshold set at 0.5 [55]. The identified contaminants were removed from dataset. After removing contaminants, all samples were rarefied to 6,000 reads per sample for downstream analysis.

Gut microbiota profiling

The bacterial DNA extraction from fecal samples of first and third batches of mice was performed as previously described [56]. A sequencing library of the V3-V4 region of the 16S rRNA gene was constructed following the manufacturer's instructions (Part # 15044223Rev.B; Illumina Inc., San Diego, CA, USA) with improvement as previously described [20], and sequenced on the Illumina MiSeq platform (Illumina, Inc., San Diego, CA, USA).

The raw paired-end reads were processed and analyzed using the QIIME2. Demultiplexed sequence data was imported into QIIME2, adapters and primers were trimmed. ASVs from each sample was inferred by using the DADA2 pipeline for filtering, dereplication, sample inference, merging of paired-end reads and chimera

identification. In the process of running the DADA2 pipeline, based on the quality profile of the data, forward and reverse reads were trimmed accordingly to ensure that the median quality score for each position is above 32. The taxonomy of all ASVs were annotated by SILVA (v132) reference database [57]. All samples were rarefied to 10,000 reads per sample for downstream analysis. Principal coordinate analysis (PCoA) of ASVs based on Bray-Curtis distance was performed using QIIME2. Subsequently the statistical significance was assessed using permutational multivariate analysis of variance (PERMANOVA) with 9,999 permutations and *P* values were adjusted for multiple comparison with Benjamini-Hochberg method [58].

Sparse partial least-squares discriminant analysis (sPLS-DA) models [59] were established to identify specific ASVs that contributed to the segregation of gut microbial structure in NC and DSS mice using "mixOmics (v6.3.1)" package [60] in R (v3.4.4). Centered log ratio (CLR) transformations of the relative abundance of ASVs were implemented in sPLS-DA models. The optimal classification performances of the sPLS-DA models were estimated by the perf function using 5-fold cross-validation with the smallest balanced error rate.

Statistical analysis

Data in point plots and bar plots, horizontal lines indicate Mean ± S.E.M. Statistical significance was assessed by Student's two-tailed t test using GraphPad Prism (version 8), with *P* values of <0.05 considered significant.

Abbreviations

IDD	Insulin-dependent diabetes
T1D	Type 1 diabetes
SCFAs	Short-chain fatty acids
DSS	Dextran sulfate sodium
OGTT	Oral glucose tolerance test
ITT	Insulin tolerance test
PCoA	Principal coordinate analysis
ASVs	Amplicon sequence variants
PERMANOVA	Permutational multivariate analysis of variance
sPLS-DA	Sparse partial least squares discriminant analysis
FISH	Fluorescence in situ hybridization
CRAMP	Cathelicidin-related antimicrobial peptide

Supplementary Information

The online version contains supplementary material available at https://doi.org/10.1186/s40168-023-01507-z.

Additional file 1: Fig. S1. Fasting C-Peptide in the mice with and without 0.2% DSS. **Fig. S2.** Serum amylase (AMS) and serum lipase levels in each group. **Fig. S3.** 0.2% DSS increased food and water intake but did not change energy intake of mice. **Fig. S4**. 0.2% DSS did not change the lipid accumulation in mice. **Fig. S5.** 0.2% DSS did not impair gut barrier integrity and induce inflammation. **Fig. S6.** qPCR of 16S rRNA gene in fecal samples. **Fig. S7.** The gut microbiota had been depleted by more than 99% in the mice with a cocktail of antibiotics for 5 weeks. **Fig. S8.** The recipient mice developed a gut microbiota more similar to their donor mice. **Fig. S9.** Optimal classification performance of the sPLS-DA model of the gut microbial structure in NC and DSS mice. **Fig. S10.** Fluorescence in situ hybridization (FISH) of 16S rRNA in the pancreas of antibiotic treated mice. **Fig. S11.** Fluorescence in situ hybridization (FISH) of 16S rRNA in the pancreas in fecal microbiota transplanted mice. **Fig. S12.** The bacterial load in the liver as measured by real-time qPCR of 16S rRNA gene. **Fig. S13.** Flow cytometry evaluation of subtypes of leukocytes in the pancreas of FM_{NC} and FM_{DSS} mice. **Fig. S14.** 0.2% DSS did not enrich bacteria in pacreas and disrupt the immune tolerance in antibiotic treated mice. **Fig. S15.** Identification of Muribaculaceae strain MF 13079. **Fig. S16.** Functional annotation of flagella-related genes and motility test of MF13079. **Fig. S17.** Bacteria load in mesenteric lymph nodes (MLN) in Akk and Muri mice. **Fig. S18.** Bray-Curtis Distance based on 16S rRNA sequencing data of gut microbiota between recipient mice and human donors. **Fig. S19**. Fluorescence in situ hybridization (FISH) of 16S rRNA in the pancreas. **Tables S1.** Culture medium used for isolation of Muribaculeae. **Table S2.** COG in the genome of MF 13079.

Acknowledgements

Not applicable.

Authors' contributions

C. Z. and L. Z. conceived, planned and supervised this study. X. Y. carried out the animal experiments and most experiments in lab. X. X. and Z. R. isolated the *Akkermansia muciniphila* strain 139 and provided the protocol of *A. muciniphila* strain 139 related animal experiment. X. Y. and J. N. performed the flow cytometry evaluation of subtypes of leukocytes in the pancreas. Y. F. and H.Y. recruited healthy subjects and T1D patients and collected fecal samples. G. W. and Z. W. provided help of genome sequencing data analysis. C. Z. and X. Y. analyzed the data and generated the figures and tables. C. Z., L. Z., J. Y., X. Y. and G. W. prepared the manuscript. All authors approved the manuscript.

Funding

This work was supported by grants from the National Key Research and Development Project (2022YFF1100103 and 2019YFA0905602) and the National Natural Science Foundation of China (31922003 and 81871091).

Availability of data and materials

The data that support the findings of this study are available from the corresponding author upon request. The 16S rRNA gene sequences of Muribaculaceae strain MF13079 has been submitted to the GenBank with the accession No. MT921595 and MT921596. The whole-genome sequence of Muribaculaceae strain MF13079 has been submitted to the NCBI under accession No. PRJNA576346.The raw Illumina sequence data generated in this study are available in the sequence read archive (SRA) at NCBI under accession No. SRP278697.

Declarations

Ethics approval and consent to participate

All experimental procedures for specific pathogen free (SPF) mice were approved by the Institutional Animal Care and Use Committee (IACUC) of the School of Life Sciences and Biotechnology of Shanghai Jiao Tong University (no. 2014005). The procedures for the germ-free mice experiments were approved by the Institutional Animal Care and Use Committee of SLAC Inc (no. 20190201001).

Consent for publication

Not applicable.

Competing interests

The authors declare no competing interests.

Received: 25 January 2023 Accepted: 25 February 2023
Published online: 29 March 2023

References

1. Petersmann A, Muller-Wieland D, Muller UA, Landgraf R, Nauck M, Freckmann G, et al. Definition, classification and diagnosis of diabetes mellitus. Exp Clin Endocrinol Diabetes. 2019;127(S 01):S1–7.
2. Beck RW, Bergenstal RM, Laffel LM, Pickup JC. Advances in technology for management of type 1 diabetes. Lancet. 2019;394(10205):1265–73.
3. Stamatouli AM, Quandt Z, Perdigoto AL, Clark PL, Kluger H, Weiss SA, et al. Collateral damage: insulin-dependent diabetes induced with checkpoint inhibitors. Diabetes. 2018;67(8):1471–80.
4. Dahlquist GG, Blom LG, Persson LA, Sandstrom AI, Wall SG. Dietary factors and the risk of developing insulin dependent diabetes in childhood. BMJ. 1990;300(6735):1302–6.
5. Chee YJ, Ng SJH, Yeoh E. Diabetic ketoacidosis precipitated by Covid-19 in a patient with newly diagnosed diabetes mellitus. Diabetes Res Clin Pract. 2020;164:108166.
6. Rewers M, Ludvigsson J. Environmental risk factors for type 1 diabetes. Lancet. 2016;387(10035):2340–8.
7. Costa FR, Francozo MC, de Oliveira GG, Ignacio A, Castoldi A, Zamboni DS, et al. Gut microbiota translocation to the pancreatic lymph nodes triggers NOD2 activation and contributes to T1D onset. J Exp Med. 2016;213(7):1223–39.
8. Vatanen T, Franzosa EA, Schwager R, Tripathi S, Arthur TD, Vehik K, et al. The human gut microbiome in early-onset type 1 diabetes from the TEDDY study. Nature. 2018;562(7728):589–94.
9. Vehik K, Lynch KF, Wong MC, Tian X, Ross MC, Gibbs RA, et al. Prospective virome analyses in young children at increased genetic risk for type 1 diabetes. Nat Med. 2019;25(12):1865–72.
10. Antvorskov JC, Halldorsson TI, Josefsen K, Svensson J, Granstrom C, Roep BO, et al. Association between maternal gluten intake and type 1 diabetes in offspring: national prospective cohort study in Denmark. BMJ. 2018;362:k3547.
11. Wen L, Ley RE, Volchkov PY, Stranges PB, Avanesyan L, Stonebraker AC, et al. Innate immunity and intestinal microbiota in the development of Type 1 diabetes. Nature. 2008;455(7216):1109–13.
12. Burrows MP, Volchkov P, Kobayashi KS, Chervonsky AV. Microbiota regulates type 1 diabetes through Toll-like receptors. Proc Natl Acad Sci U S A. 2015;112(32):9973–7.
13. Markle JG, Frank DN, Mortin-Toth S, Robertson CE, Feazel LM, Rolle-Kampczyk U, et al. Sex differences in the gut microbiome drive hormone-dependent regulation of autoimmunity. Science. 2013;339(6123):1084–8.
14. Candon S, Perez-Arroyo A, Marquet C, Valette F, Foray AP, Pelletier B, et al. Antibiotics in early life alter the gut microbiome and increase disease incidence in a spontaneous mouse model of autoimmune insulin-dependent diabetes. PloS One. 2015;10(5):e0125448.
15. Livanos AE, Greiner TU, Vangay P, Pathmasiri W, Stewart D, McRitchie S, et al. Antibiotic-mediated gut microbiome perturbation accelerates development of type 1 diabetes in mice. Nat Microbiol. 2016;1(11):16140.
16. Sun J, Furio L, Mecheri R, van der Does AM, Lundeberg E, Saveanu L, et al. Pancreatic beta-cells limit autoimmune diabetes via an immunoregulatory antimicrobial peptide expressed under the influence of the gut microbiota. Immunity. 2015;43(2):304–17.
17. Wu QL, Chen TT, El-Nezami H, Savidge TC. Food ingredients in human health: Ecological and metabolic perspectives implicating gut microbiota function. Trends Food Sci Technol. 2020;100:103–17.
18. Chassaing B, Srinivasan G, Delgado MA, Young AN, Gewirtz AT, Vijay-Kumar M. Fecal lipocalin 2, a sensitive and broadly dynamic non-invasive biomarker for intestinal inflammation. PloS One. 2012;7(9):e44328.
19. Okamoto T, Sasaki M, Tsujikawa T, Fujiyama Y, Bamba T, Kusunoki M. Preventive efficacy of butyrate enemas and oral administration of Clostridium butyricum M588 in dextran sodium sulfate-induced colitis in rats. J Gastroenterol. 2000;35(5):341–6.
20. Zhang Q, Wu Y, Wang J, Wu G, Long W, Xue Z, et al. Accelerated dysbiosis of gut microbiota during aggravation of DSS-induced colitis by a butyrate-producing bacterium. Sci Rep. 2016;6:27572.
21. Sorini C, Cosorich I, Lo Conte M, De Giorgi L, Facciotti F, Luciano R, et al. Loss of gut barrier integrity triggers activation of islet-reactive T cells and autoimmune diabetes. Proc Natl Acad Sci U S A. 2019;116(30):15140–9.
22. Lundberg R, Toft MF, August B, Hansen AK, Hansen CH. Antibiotic-treated versus germ-free rodents for microbiota transplantation studies. Gut Microbes. 2016;7(1):68–74.
23. Lagkouvardos I, Lesker TR, Hitch TCA, Galvez EJC, Smit N, Neuhaus K, et al. Sequence and cultivation study of Muribaculaceae reveals novel species, host preference, and functional potential of this yet undescribed family. Microbiome. 2019;7(1):28.
24. Chen J, Vitetta L. The Role of Butyrate in Attenuating Pathobiont-Induced Hyperinflammation. Immune Netw. 2020;20(2):e15.
25. Thomas RM, Jobin C. Microbiota in pancreatic health and disease: the next frontier in microbiome research. Nat Rev Gastroenterol Hepatol. 2020;17(1):53–64.
26. Torchinsky MB, Garaude J, Martin AP, Blander JM. Innate immune recognition of infected apoptotic cells directs T(H)17 cell differentiation. Nature. 2009;458(7234):78–82.
27. Cebula A, Seweryn M, Rempala GA, Pabla SS, McIndoe RA, Denning TL, et al. Thymus-derived regulatory T cells contribute to tolerance to commensal microbiota. Nature. 2013;497(7448):258–62.
28. Tindall BJ, Rossello-Mora R, Busse HJ, Ludwig W, Kampfer P. Notes on the characterization of prokaryote strains for taxonomic purposes. Int J Syst Evol Microbiol. 2010;60(Pt 1):249–66.
29. Ha CWY, Martin A, Sepich-Poore GD, Shi B, Wang Y, Gouin K, et al. Translocation of viable gut microbiota to mesenteric adipose drives formation of creeping fat in humans. Cell. 2020;183(3):666–683 e617.
30. Zhai R, Xue X, Zhang L, Yang X, Zhao L, Zhang C. Strain-specific anti-inflammatory properties of two akkermansia muciniphila strains on chronic colitis in mice. Front Cell Infect Microbiol. 2019;9:239.
31. Diehl GE, Longman RS, Zhang JX, Breart B, Galan C, Cuesta A, et al. Microbiota restricts trafficking of bacteria to mesenteric lymph nodes by CX(3)CR1(hi) cells. Nature. 2013;494(7435):116–20.
32. Bravo-Blas A, Utriainen L, Clay SL, Kastele V, Cerovic V, Cunningham AF, et al. Salmonella enterica serovar typhimurium travels to mesenteric lymph nodes both with host cells and autonomously. J Immunol. 2019;202(1):260–7.
33. Ormerod KL, Wood DL, Lachner N, Gellatly SL, Daly JN, Parsons JD, et al. Genomic characterization of the uncultured Bacteroidales family S24-7 inhabiting the guts of homeothermic animals. Microbiome. 2016;4(1):36.
34. Smith BJ, Miller RA, Schmidt TM. Muribaculaceae genomes assembled from metagenomes suggest genetic drivers of differential response to acarbose treatment in mice. mSphere. 2021;6(6):e0085121.
35. Park JK, Chang DH, Rhee MS, Jeong H, Song J, Ku BJ, et al. Heminiphilus faecis gen. nov., sp. nov., a member of the family Muribaculaceae, isolated from mouse faeces and emended description of the genus Muribaculum. Antonie Van Leeuwenhoek. 2021;114(3):275–86.
36. Zhang XS, Li J, Krautkramer KA, Badri M, Battaglia T, et al. Antibiotic-induced acceleration of type 1 diabetes alters maturation of innate intestinal immunity. eLife. 2018;7:e37816.
37. Vecchio F, Messina G, Giovenzana A, Petrelli A. New evidence of exocrine pancreatopathy in pre-symptomatic and symptomatic type 1 diabetes. Curr Diab Rep. 2019;19(10):92.
38. Ahuja M, Schwartz DM, Tandon M, Son A, Zeng M, Swaim W, et al. Orai1-mediated antimicrobial secretion from pancreatic acini shapes the gut microbiome and regulates gut innate immunity. Cell Metab. 2017;25(3):635–46.
39. Zhao L, Zhang F, Ding X, Wu G, Lam YY, Wang X, et al. Gut bacteria selectively promoted by dietary fibers alleviate type 2 diabetes. Science. 2018;359(6380):1151–6.
40. Rakoff-Nahoum S, Paglino J, Eslami-Varzaneh F, Edberg S, Medzhitov R. Recognition of commensal microflora by toll-like receptors is required for intestinal homeostasis. Cell. 2004;118(2):229–41.
41. Zou Y, Xue W, Luo G, Deng Z, Qin P, Guo R, et al. 1,520 reference genomes from cultivated human gut bacteria enable functional microbiome analyses. Nat Biotechnol. 2019;37(2):179–85.
42. Zhang C, Yin A, Li H, Wang R, Wu G, Shen J, et al. Dietary modulation of gut microbiota contributes to alleviation of both genetic and simple obesity in children. EBioMedicine. 2015;2(8):968–84.
43. Alberti KG, Zimmet PZ. Definition, diagnosis and classification of diabetes mellitus and its complications. Part 1: diagnosis and classification of diabetes mellitus provisional report of a WHO consultation. Diabet Med. 1998;15(7):539–53.
44. Plovier H, Everard A, Druart C, Depommier C, Van Hul M, Geurts L, et al. A purified membrane protein from Akkermansia muciniphila or the pasteurized bacterium improves metabolism in obese and diabetic mice. Nat Med. 2017;23(1):107–13.

45. Zaki MH, Boyd KL, Vogel P, Kastan MB, Lamkanfi M, Kanneganti TD. The NLRP3 inflammasome protects against loss of epithelial integrity and mortality during experimental colitis. Immunity. 2010;32(3):379–91.
46. Roch AM, Maatman TK, Cook TG, Wu HH, Merfeld-Clauss S, Traktuev DO, et al. Therapeutic use of adipose-derived stromal cells in a murine model of acute pancreatitis. J Gastrointest Surg. 2020;24(1):67–75.
47. Wang CJ, Zhou ZG, Holmqvist A, Zhang H, Li Y, Adell G, et al. Survivin expression quantified by Image Pro-Plus compared with visual assessment. Appl Immunohistochem Mol Morphol. 2009;17(6):530–5.
48. Chin CS, Alexander DH, Marks P, Klammer AA, Drake J, Heiner C, et al. Nonhybrid, finished microbial genome assemblies from long-read SMRT sequencing data. Nat Methods. 2013;10(6):563–9.
49. Seemann T. Prokka: rapid prokaryotic genome annotation. Bioinformatics. 2014;30(14):2068–9.
50. Nadkarni MA, Martin FE, Jacques NA, Hunter N. Determination of bacterial load by real-time PCR using a broad-range (universal) probe and primers set. Microbiology (Reading). 2002;148(Pt 1):257–66.
51. Sunde PT, Olsen I, Gobel UB, Theegarten D, Winter S, Debelian GJ, et al. Fluorescence in situ hybridization (FISH) for direct visualization of bacteria in periapical lesions of asymptomatic root-filled teeth. Microbiology (Reading). 2003;149(Pt 5):1095–102.
52. Thimm T, Tebbe CC. Protocol for rapid fluorescence in situ hybridization of bacteria in cryosections of microarthropods. Appl Environ Microbiol. 2003;69(5):2875–8.
53. Choi YS, Kim YC, Baek KJ, Choi Y. In situ detection of bacteria within paraffin-embedded tissues using a digoxin-labeled DNA probe targeting 16S rRNA. J Vis Exp. 2015;99:e52836.
54. Callahan BJ, McMurdie PJ, Rosen MJ, Han AW, Johnson AJ, Holmes SP. DADA2: High-resolution sample inference from Illumina amplicon data. Nat Methods. 2016;13(7):581–3.
55. Davis NM, Proctor DM, Holmes SP, Relman DA, Callahan BJ. Simple statistical identification and removal of contaminant sequences in marker-gene and metagenomics data. Microbiome. 2018;6(1):226.
56. Godon JJ, Zumstein E, Dabert P, Habouzit F, Moletta R. Molecular microbial diversity of an anaerobic digestor as determined by small-subunit rDNA sequence analysis. Appl Environ Microbiol. 1997;63(7):2802–13.
57. Quast C, Pruesse E, Yilmaz P, Gerken J, Schweer T, Yarza P, et al. The SILVA ribosomal RNA gene database project: improved data processing and web-based tools. Nucleic Acids Res. 2013;41(Database issue):D590–6.
58. Anderson MJ. A new method for non-parametric multivariate analysis of variance. Austral Ecol. 2001;26(1):32–46.
59. Le Cao KA, Boitard S, Besse P. Sparse PLS discriminant analysis: biologically relevant feature selection and graphical displays for multiclass problems. BMC Bioinformatics. 2011;12:253.
60. Rohart F, Gautier B, Singh A, Le Cao KA. mixOmics: an R package for 'omics feature selection and multiple data integration. PLoS Comput Biol. 2017;13(11):e1005752.

Publisher's Note